AD-A109 718 SYSTEMS SCIENCE AND SOFTWARE LA JOLLA CA F/G 18/3
THE RELATIONSHIP BETWEEN MATERIAL PROPERTIES, RESIDUAL STRESSES--ETC(U)
MAY 76 N RIMER DNA001-76-C-0072
UNCLASSIFIED SSS-R-76-2907 DNA-5864T NL

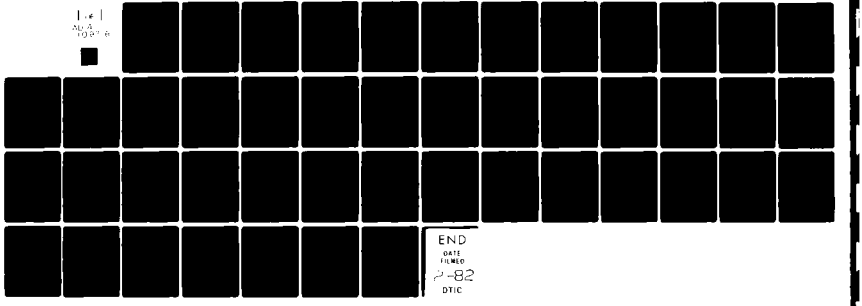

END
DATE FILMED
2-82
DTIC

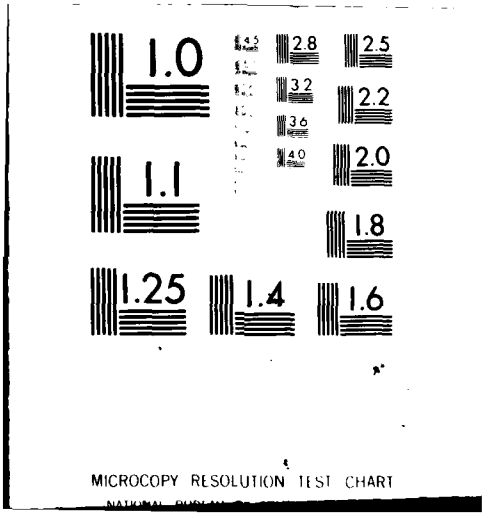
1.0
2.8
2.5
3.2
2.2
3.6
4.0
2.0
1.1
1.8
1.25
1.4
1.6
MICROCOPY RESOLUTION TEST CHART

(12)

DNA 5864T

THE RELATIONSHIP BETWEEN MATERIAL PROPERTIES, RESIDUAL STRESSES AND CAVITY RADIUS DUE TO A NUCLEAR EXPLOSION

N. Rimer
Systems, Science and Software, Inc.
P.O. Box 1620
La Jolla, California 92038

1 May 1976

Topical Report for Period 26 September 1975—1 May 1976

CONTRACT No. DNA 001-76-C-0072

APPROVED FOR PUBLIC RELEASE;
DISTRIBUTION UNLIMITED.

THIS WORK SPONSORED BY THE DEFENSE NUCLEAR AGENCY
UNDER RDT&E RMSS CODE B34507T462 J24AAXYX98330 H2590D.

Prepared for
Director
DEFENSE NUCLEAR AGENCY
Washington, D. C. 20305

Destroy this report when it is no longer needed. Do not return to sender.

PLEASE NOTIFY THE DEFENSE NUCLEAR AGENCY, ATTN: STTI, WASHINGTON, D.C. 20305, IF YOUR ADDRESS IS INCORRECT, IF YOU WISH TO BE DELETED FROM THE DISTRIBUTION LIST, OR IF THE ADDRESSEE IS NO LONGER EMPLOYED BY YOUR ORGANIZATION.

UNCLASSIFIED

SECURITY CLASSIFICATION OF THIS PAGE (When Data Entered)

REPORT DOCUMENTATION PAGE	READ INSTRUCTIONS BEFORE COMPLETING FORM
1. REPORT NUMBER: DNA 5864T	2. GOVT ACCESSION NO.: AD-A109 718
3. RECIPIENT'S CATALOG NUMBER:	
4. TITLE (and Subtitle): THE RELATIONSHIP BETWEEN MATERIAL PROPERTIES, RESIDUAL STRESSES AND CAVITY RADIUS DUE TO A NUCLEAR EXPLOSION	5. TYPE OF REPORT & PERIOD COVERED: Topical Report for Period 26 Sep 75—1 May 76
	6. PERFORMING ORG. REPORT NUMBER: SSS-R-76-2907
7. AUTHOR(s): Dr. Norton Rimer	8. CONTRACT OR GRANT NUMBER(s): DNA 001-76-C-0072
9. PERFORMING ORGANIZATION NAME AND ADDRESS: Systems, Science & Software, Inc. P. O. Box 1620 La Jolla, California 92038	10. PROGRAM ELEMENT, PROJECT, TASK AREA & WORK UNIT NUMBERS: Subtask J24AAXYX983-30
11. CONTROLLING OFFICE NAME AND ADDRESS: Director Defense Nuclear Agency Washington, DC 20305	12. REPORT DATE: 1 May 1976
	13. NUMBER OF PAGES: 46
14. MONITORING AGENCY NAME & ADDRESS (if different from Controlling Office)	15. SECURITY CLASS. (of this report): UNCLASSIFIED
	15a. DECLASSIFICATION/DOWNGRADING SCHEDULE: N/A

16. DISTRIBUTION STATEMENT (of this Report)

Approved for public release; distribution unlimited.

17. DISTRIBUTION STATEMENT (of the abstract entered in Block 20, if different from Report)

18. SUPPLEMENTARY NOTES

This work sponsored by the Defense Nuclear Agency under RDT&E RMSS Code B34507T462 J24AAXYX98330 H2590D.

19. KEY WORDS (Continue on reverse side if necessary and identify by block number)

Ground Shock
Residual Stresses
Cavity Radius
Failure Surface

20. ABSTRACT (Continue on reverse side if necessary and identify by block number)

The influence of material properties on the magnitude of the residual stresses around a nuclear cavity is examined. Particular attention in given to the effect on peak transverse residual stresses of parametrically varying material properties such as water content, percentage of air-filled voids, elastic properties, shear strength and depth of burial. The influence of these parametric variations on the final cavity radius is discussed. A → cont

DD FORM 1 JAN 73 1473 EDITION OF 1 NOV 65 IS OBSOLETE

UNCLASSIFIED

SECURITY CLASSIFICATION OF THIS PAGE (When Data Entered)

20. (Continued)

correlation between peak residual stress and cavity radius is noted; a larger cavity radius implies a smaller residual stress.

TABLE OF CONTENTS

LIST OF ILLUSTRATIONS

1. INTRODUCTION AND SUMMARY

A calculational parameter study is presented here of the effects of material properties upon the magnitude of compressive explosion-induced residual stresses around the cavity produced by a nuclear explosion. Recent hydrofracture measurements by W. Ellis[1] of the U.S. Geological Survey around the Hybla Fair cavity show that the rock has been noticeably strengthened by the event. It is believed that these compressive residual stresses are of primary importance in the containment of the hot cavity gases. Static two-dimensional finite element calculations discussed by Duff, et al.[2] indicate that the compressive residual stress field greatly increases the resistance of the rock to tensile hydrofracture.

This parameter study involves an analysis of the existing near field ground motion calculations at S^3 and, in particular, the late-time calculations made in connection with the teleseismic program of Dr. Cherry. Since only three calculations were made directly for this study, it is incomplete in some areas. Some of the calculations presented have also been discussed in a previous report by Rimer.[3] However, attention is given here to the transverse residual stresses and to the final cavity radius rather than to the peak radial residual stresses. Also, the results of many more calculations, not available previously, are presented to fill in some of the gaps left from the first report.

In the first report, an analogy was made between the residual stresses formed by the torsion of a solid steel shaft or the bending of a beam and the residual stresses around a nuclear cavity. It was hypothesized that residual stresses are caused by nonuniform loading into the plastic regime. When the material unloads, stresses result between elastic

elements, which cannot recover all of their deformation. Any change in material property which tends to increase the relative deformation between elements therefore increases these residual stresses.

The results of this parameter study tend to corroborate the above argument. Some of these results are:

(1) Increasing the shear strength of the material increases the magnitude of the residual stresses. The stress magnitudes are particularly sensitive to the shear strength at low pressure (unconfined strength, etc.).

(2) Since increased depth of burial increases the yield strength (for the modeling used), it also increases the residual stresses.

(3) Increased shear modulus increases residual stresses.

(4) A material which is stronger in tension will have lower residual stresses. This surprising result follows directly from the above arguments, since tensile fracturing increases the nonuniformity of the stress distribution.

(5) Air-filled voids act as a smoothing (dispersive) mechanism which reduces the nonuniformity of the loading and therefore reduces residual stresses.

(6) Cavity radius varies inversely as peak residual stresses for the material properties studied.

(7) The numerical treatment of the cavity source (as distinct from equation of state of the cavity) can influence both residual stress and cavity radius. The cavity treatment used in some of the older calculations presented in this report (and a recent Pacifica Technology parameter study) vs more recent cavity treatment is discussed here.

2. THE EFFECT OF MATERIAL PROPERTIES ON RESIDUAL STRESSES

Figure 1 shows the radial and tangential residual stresses *vs* position (compressive stresses are shown positive) for a SKIPPER calculation using Husky Ace material properties (see Rimer, *et al.*[4]) for a nominal yield of 20 tons. These profiles correspond to calculation HA14 in Table 1 and are fairly typical of the distribution of residual stress given by calculations. All stresses shown in Table 1 are relative to a hydrostatic overburden pressure. The radial stresses in Figure 1 resist a cavity pressure (greater than overburden), increase with position to some peak value and gradually decrease to zero. The peak transverse stress is generally greater in magnitude and occurs closer to the cavity than the radial peak. However, these transverse stresses decay rapidly with position, eventually becoming tensile. Thus, the region of compressive transverse stresses, which are believed to prevent radial tensile cracks from forming around the cavity, is relatively small.

In this section, the effect of calculational variations in material properties on the peak value of transverse residual stress is examined. Table 1 summarizes the material properties of interest and the resulting peak radial and transverse residual stresses as well as the cavity radii for a nominal 20 ton yield. Calculations are identified mnemonically as follows: H1-H11 and H25-H31 refer to a study by J. T. Cherry[5] of the influence of the material properties of a tuff on teleseismic coupling, HR32-HR37 to a more recent study (see Cherry[6]) of the effect of water content, those labeled HZ to the same study, the letter Z referring to a different model for the cavity source. Calculations 13-18 refer to specific NTS events detonated in Area 12 tuff, HA to Husky Ace, DS to Diamond Sculls, DQ to Dido Queen, and MN to Misty North. These calculations are discussed in

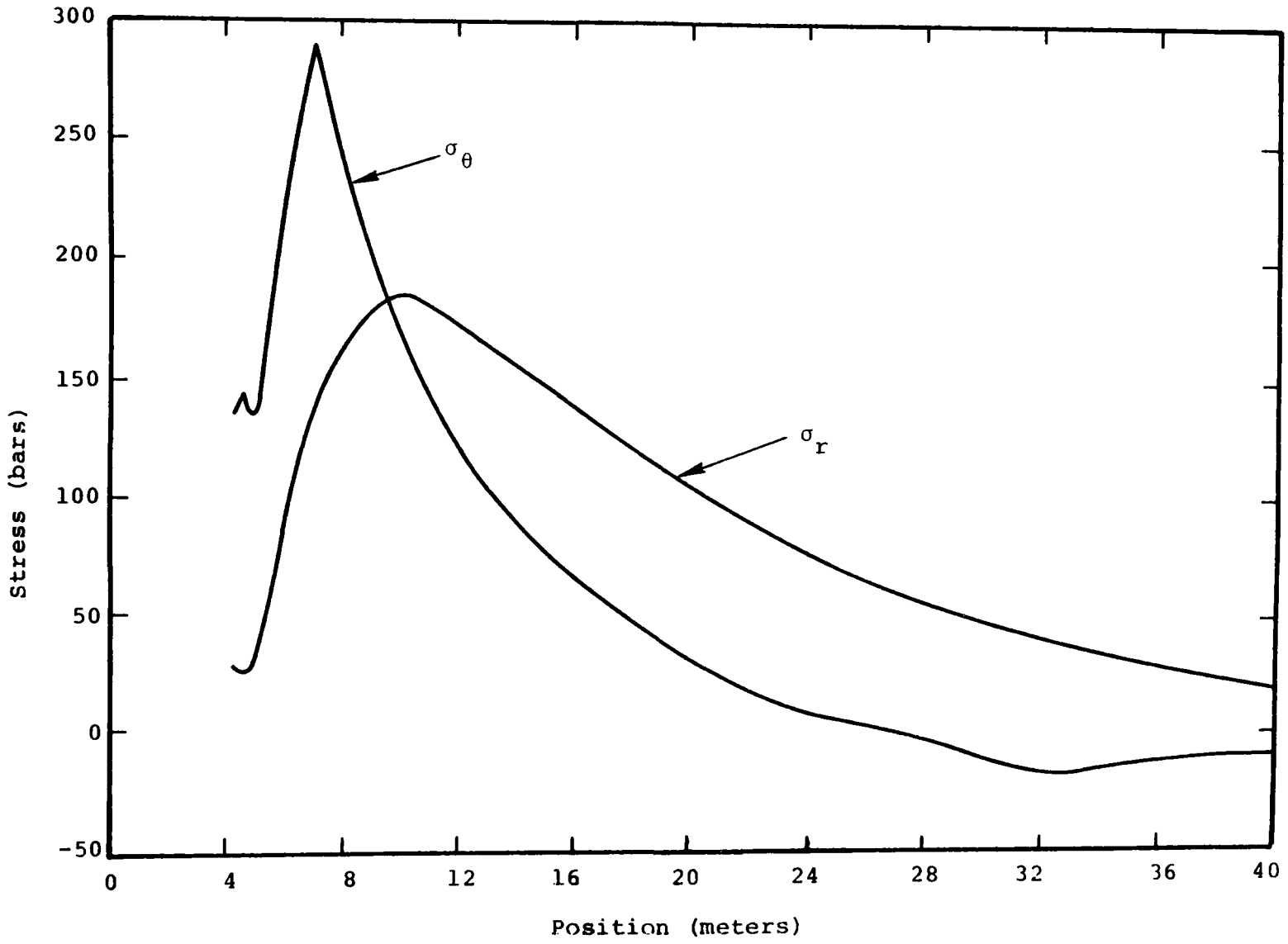

Figure 1 - Radial and tangential residual stress vs final position for Husky Ace material properties.

Table 1

Material properties for the parameter study

ID	Density (gm/cc)	Water content	Air-filled voids	Sound speed (km/sec)	Over-burden (bars)	Shear modulus (kbars)	Maximum yield strength (kbars)	Cohesive strength (kbars)	Pressure for max. strength (kbars)	Melt energy 10^{10} ergs/gm	Crush pressure (kbars)	Elastic pressure (kbars)	Radial residual stress (bars)	Hoop residual stress (bars)	Cavity radius 20 ton yield (m)
H1	1.94	0.17	0	2.4	116	40	0.5	0	0.6	1.5	0	0	340	606	3.41
H2	1.94	0.17	0	2.4	40	40	0.5	0	0.6	1.5	0	0	200	293	3.80
H3	1.84	0.17	0.05	1.7	116	20	0.5	0	0.6	1.5	1.25	0.15	380	622	3.57
H4	1.84	0.17	0.05	1.7	40	20	0.5	0	0.6	1.5	1.25	0.15	196	292	4.08
H5	1.84	0.17	0.05	2.4	116	40	0.5	0	0.6	1.5	1.25	0.15	395	615	3.52
H6	1.84	0.17	0.05	2.4	116	40	0.5	0	0.6	1.5	0.5	0.075	332	532	3.64
						Poisson ratio=									
H7	1.84	0.17	0.05	2.4	116	0.197	0.5	0	0.6	1.5	0.5	0.075	338	509	3.67
H8	1.90	0.17	0.02	2.4	116	40	0.5	0	0.6	1.5	0.5	0.075	375	591	3.60
H9	2.28	0	0.05	2.4	116	40	0.5	0	0.6	1.5	0.5	0.075	386	642	3.89
H10	2.28	0	0.05	1.7	40	20	0.5	0	0.6	1.5	1.25	0.15	236	434	4.25
H11	1.90	0.17	0.02	2.4	75	40	0.5	0	0.6	1.5	0.5	0.075	300	479	3.78
H12	1.90	0.17	0.02	2.4	348	40	0.5	0	0.6	1.5	0.5	0.075	665	909	2.98
HA13	1.91	0.17	0.012	2.34	56	35.7	0.45	0	1.25	3.2	1.5	0.05	96	166	4.55
HA14	1.91	0.17	0.012	2.34	56	35.7	0.18	0.0553	0.4	3.2	1.5	0.05	180	292	4.32
DS15	1.98	0.136	0.016	2.59	56	10.4	0.31	0.06	0.4	3.2	1.5	0.05	135	313	4.12
DQ16	1.91	0.17	0.016	2.59	56	10.5	0.18	0.0553	0.4	3.2	1.5	0.05	144	241	4.54
DQ17	1.91	0.17	0.016	2.59	56	54	0.18	0.0553	0.4	3.2	1.5	0.05	216	404	4.31
WN18	1.87	0.19	0.016	2.75	56	17	0.45	0	1.25	3.2	1.5	0.05	104	142	4.69
WF19	1.70	0.136	0.1564	2.13	96	25.8	0.62	0.12	0.4	3.2	4.36	0.18	344	714	3.53
S20	2.21	0.19	0	2.36	0	30.8	0.2	0.05	0.2	3.2	0	0	130	280	
S21	2.21	0.19	0	2.36	0	30.8	0.5	0.05	0.4	3.2	0	0	175	262	3.51
S22	2.21	0.19	0	2.36	116	30.8	0.5	0.05	0.4	3.2	0	0	500	702	
S23	2.21	0.19	0	2.36	0	30.8	0.5	0.05	0.4	3.2	0	0	340	580	3.82
	Tensile strength = 10 bars														
S24	2.21	0.19	0	2.36	0	30.8	0.5	0.05	0.4	3.2	0	0	390	603	3.79
	Tensile strength = 5 bars														
H25	1.84	0.17	0.05	1.7	40	20	0.5	0	0.6	1.5	0.5	0.075	198	336	
H26	1.90	0.17	0.02	2.4	619	40	0.5	0	0.6	1.5	0.5	0.075	922	1173	2.61
H27	1.90	0.17	0.02	2.4	75	40	0.5	0	0.6	1.5	1.25	0.075	322	499	3.68
H28	1.84	0.17	0.05	2.4	116	40	1.5	0	0.6	1.5	0.5	0.075	443	766	2.79
H29	1.84	0.17	0.05	2.4	247	40	1.0	0	0.6	1.5	0.5	0.075	456	785	2.88
H30	1.84	0.17	0.05	2.4	116	40	1.0	0	0.6	1.5	0.5	0.075	467	646	3.10
H31	1.84	0.17	0.05	2.4	179	40	1.0	0	0.6	1.5	0.5	0.075	417	714	2.99
HR32	1.89	0.19	0	2.38	116	40	0.5	0	0.6	3.2	0	0	332	567	3.40
HR33	1.94	0.17	0	2.40	116	40	0.5	0	0.6	3.2	0	0	329	564	3.40
HR34	2.02	0.136	0	2.44	116	40	0.5	0	0.6	3.2	0	0	348	563	3.40
HR35	2.24	0.05	0	2.79	116	40	0.5	0	0.6	3.2	0	0	289	458	3.44
HR36	2.40	0	0	3.81	116	40	0.5	0	0.6	3.2	0	0	355	600	3.66
LR37	1.94	0.17	0	2.40	116	40	0.5	0	0.6	1.5	0	0	340	606	3.41
HAZ38	1.91	0.17	0.012	2.34	56	35.7	0.18	0.0553	0.4	3.2	1.5	0.05	202	295	4.33
HAZ39	1.91	0.17	0.012	2.34	56	35.7	0.40	0.0553	0.4	3.2	1.5	0.05	303	448	4.03
HR740	2.24	0.05	0	2.79	116	40	0.5	0	0.6	3.2	0	0	328	583	3.81
HZ41	1.84	0.17	0.05	2.4	116	40	1.0	0	0.6	2.0	0.5	0.075	449	642	3.52
HZ42	1.84	0.17	0.05	2.4	116	40	0.75	0	0.6	2.0	0.5	0.075	317	497	3.77
HZ43	1.84	0.17	0.05	2.4	116	40	0.9	0.1	0.6	2.0	0.5	0.075	474	696	3.49
HZ44	1.84	0.17	0.05	2.4	116	40	0.8	0.2	0.6	2.0	0.5	0.075	500	760	3.47
HZ45	1.84	0.17	0.05	2.4	116	40	0	1.0	0.6	2.0	0.5	0.075	590	866	3.24
HZ46	1.84	0.17	0.05	2.4	116	40	1.0	0	0.6	2.0	0.5	0.15	426	709	3.49
HZ47	1.84	0.17	0.05	2.32	116	40	1.0	0	0.6	2.0	0.5	0.075	446	651	3.53
HZ48	1.84	0.17	0.05	2.25	116	40	1.0	0	0.6	2.0	0.5	0.075	444	652	3.54
HZ49	1.84	0.17	0.05	2.40	116	42	1.0	0	0.6	2.0	0.5	0.075	447	641	3.52
HZ50	1.84	0.17	0.05	2.40	116	45	1.0	0	0.6	2.0	0.5	0.075	441	631	3.52
HZ51	1.94	0.17	0	2.4	116	40	0.5	0	0.6	3.2	0	0	348	547	3.80
HA52	1.91	0.17	0.012	2.34	56	35.7	0.45	0	1.25	3.2	1.5	0.05	98	169	4.46
HR53	2.13	0.05	0.05	2.80	116	40	0.5	0	0.6	1.5	0.5	0.075	225	430	3.74
HR54	2.185	0.07	0	2.65	116	40	0.5	0	0.6	3.2	0	0	319	567	3.43
HR55	2.30	0.03	0	3.02	116	40	0.5	0	0.6	3.2	0	0	260	460	3.465

Rimer, et al.[4] YF19 refers to a Yucca Flat dry tuff simulation discussed in Bache, et al.[7] Calculations S20-S24, in shale, are discussed in Rimer.[3]

2.1 CAVITY SOURCE MODELING

Calculations numbered 1 through 18, 25 through 37, 53 through 55, and a similar parameter study by Pacifica Technology (see R. Allen[8]) used a cavity source model which, for purposes of this discussion, will be referred to as the ramping source. This source introduces a cavity pressure boundary condition to drive the SKIPPER calculation. The cavity pressur is computed using an ideal gas equation of state given by

$$P_c = \frac{4.186 \times 10^{19} \, W(\gamma-1)}{\frac{4}{3}\pi R_o^3} \left(\frac{R_o}{R(1)}\right)^{3\gamma} \text{(dynes/cm}^2\text{)} \qquad (1)$$

where

W = device yield (Kilotons)

R_o = initial cavity radius (cm)

$R(1)$ = cavity radius (cm) at time t

γ = ratio of specific heats.

The cavity pressure is "ramped," i.e., restrained to build up slowly for the first 50 to 100 cycles by modifying the above equation as follows

$$P = P_c \frac{t}{t_o} \qquad P \leq P_c \qquad (2)$$

where t_o is the time it would take for a wave propagating at the sound speed of the cavity material at time t to propagate through 4 zones. Ramping is discontinued and Equation (1) is

used when t remains greater than t_o for 20 consecutive cycles. This is, of course, artificial.

The original purpose of this ramping source model is related to the Tabular Arrays of Mixtures Equation of State (TAMEOS), described later in this report. The original TAMEOS table used in the calculations only reached to a maximum pressure of 600 kbars. Ramping was used to avoid having the pressure in the first grid zone outside the cavity exceed the bounds of the table. When tables were developed reaching to higher maximum pressures, ramping was no longer needed. However, in order to compare older with newer calculations, the ramping model was retained far longer than necessary.

The ramping source model has many disadvantages, the most important being that it is nonconservative during the ramping phase. The amount of ramping and therefore the energy loss is dependent upon the zoning used in the calculation (t_o depends on zoning). Energy losses of 10 to 15 percent have been observed in the calculations presented in this report. However, losses of 40 to 50 percent have been seen in calculations in sand (40 percent air-filled voids). R. Bjork[9] considers the energy remaining in the calculation after the ramping phase to be the actual device yield of the calculation. This is probably the best approach to use, but does not eliminate the difficulty associated with ramping. Comparisons presented in this section indicate that cavity radii obtained with and without ramping differ by far more than the energy lost (using $W^{1/3}$ scaling). This is also true of reduced displacement potentials (RDP), measures of the coupling efficiency of elastic waves from a device into the ground. The RDP scales with yield and increases by approximately 35 percent when ramping is not used.

As a first step toward improving the cavity representation, the so-called "bubble" model (see Schroeder[10]) was

incorporated into SKIPPER. This model assumes that 70 metric tons of rock at ambient density is vaporized for each Kiloton of nuclear explosive in order to compute an initial cavity radius. The device energy is loaded into the cavity which is modeled using one grid zone with an ideal gas equation of state with constant γ of 1.5. This procedure results in energy conservation to better than one percent in all calculations. In this report, calculations 19-24 and 38-51 were made using this cavity model. More recent work on a cavity equation of state by D. Laird[11] indicates that γ varies from approximately 1.55 at zero time to 1.1 at later times. Since the influence of the cavity at early times is far more important to the wave propagation, the choice of $\gamma = 1.5$ seems reasonable as a first approximation.

Calculations 1 through 12 and 25 through 37 and HA52 for the ramping source model used $\gamma = 4/3$ for the source material, while 13 through 18 used $\gamma = 1.5$. All used an arbitrary initial cavity radius which is equivalent to vaporizing approximately 35 tons per Kiloton of explosive. Comparisons between the bubble model and the ramping source may be made from Table 1. Three comparisons are reproduced in Table 2, each pair for identical material properties outside the cavity source. In all cases, the bubble model used $\gamma = 1.5$ in the cavity (γ for the ramping model varied). The results of calculations HA13 for $\gamma = 1.5$ and HA52 for $\gamma = 4/3$, which have identical material properties, show that at least for the ramping source model, the value of γ has negligible influence on residual stresses. The larger γ did increase the cavity radius by about 2 percent. Due to the apparent small effect of changing γ, the variation in γ in Table 2 will be ignored.

Comparisons 1 and 2 indicate only slight differences in residual stresses. Cavity radii for the bubble model are

Table 2

Comparisons of source modeling

Comparison No.	1		2		3	
	Ramping	Bubble	Ramping	Bubble	Ramping	Bubble
ID	HA14	HAZ38	HR33	HZ51	HR35	HRZ40
γ	1.5	1.5	4/3	1.5	4/3	1.5
Cavity radius (m)	4.32	4.83	3.40	3.80	3.44	3.83
Radial residual stress (bars)	180	202	329	348	289	328
Transverse residual stress (bars)	292	295	588	610	480	584

approximately 12 percent greater in both cases. A similar increase in cavity radius is seen in comparison 3. However, unlike the first two comparisons, residual stresses show significant increases for the bubble calculation.

Summarizing, the bubble cavity source model is an improvement over the ramping source model which is nonconservative. The bubble model leads to larger cavity radii; however, further work is needed to determine the effect of cavity modeling on peak residual stresses. For the parameter study to be presented in this report, comparisons between calculations having different cavity source models will be avoided.

2.2 WATER CONTENT AND AIR-FILLED VOIDS

All calculations presented except S20 through S24 utilize the TAMEOS tabular equation of state for tuff. A TAMEOS table is generated for a given water content (mass fraction of water) assuming zero air-filled porosity. The table describes all relevant states of the mixture of dry (crystalline) tuff of grain density 2.4, represented by an equation of state of the Mie-Gruneisen type and water, represented by an equation of state developed by Bjork.[12] The TAMEOS scheme, described in Riney, et al.,[13] assumes pressure equilibrium between the dry tuff and water.

The air-filled voids are included through the S^3 constitutive equation for porous materials (P-α model) shown graphically in Figure 2. The pressure of the porous material is described by

$$P = \left(\frac{1}{\alpha}\right) \bar{P} \left(\frac{v}{\alpha}, e\right) \tag{3}$$

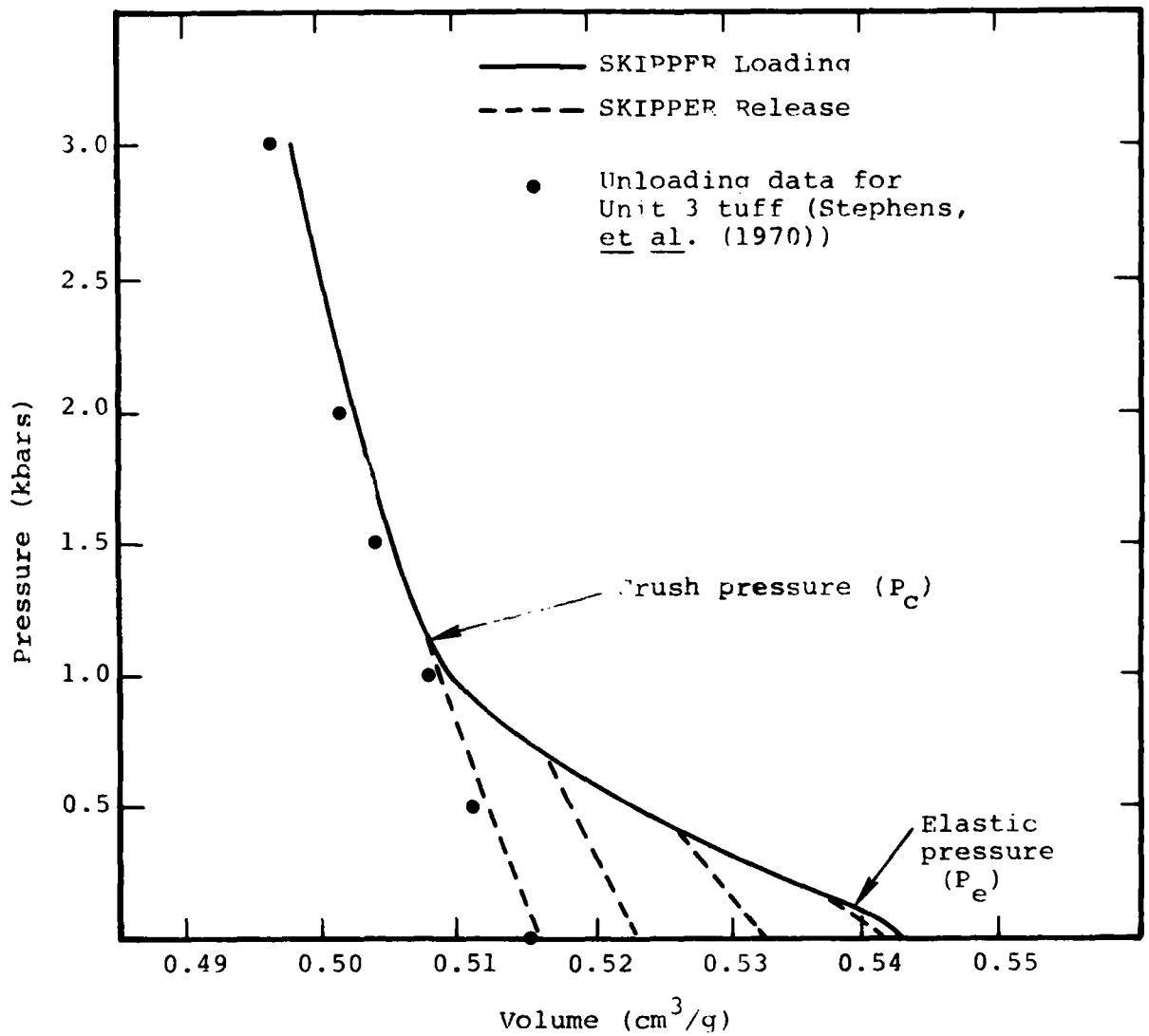

Figure 2 - Loading and release p-V curves for partially saturated tuff (f = 0.17, ϕ_o = 0.05) [Cherry, et al.[5]]

where

v = specific volume of the material
e = specific internal energy
$\bar{P}$ = pressure obtained from the TAMEOS table
α = distension ration defined by

$$\alpha = \left(\frac{v}{\bar{v}}\right) \geq 1 \qquad (4)$$

where $\bar{v}$ is the specific volume of the material with zero air-filled voids. The distension ratio is required to decrease from an initial value at zero pressure down to 1.0 as the pressure increases to P_c, the crush pressure at which all air-filled porosity is irreversibly removed. The pressure limit for the completely reversible portion of the void collapse P_e, locates the boundary between two functions $\alpha(v)$, elastic and plastic, which together define the crush curve. Unloading from the plastic portion of the curve allows for partial pore recovery in order to provide continuity at P_e. Thus, the dotted curves in Figure 2 are not parallel.

Figure 3 shows the effect of water content on the peak value of transverse residual stress. Each curve has all material properties except water content held constant, the numbers on a curve representing the corresponding calculation numbers in Table 1. Where a curve consists of only two data points, they are joined by a straight line. This is not intended to imply a straight line relationship. In fact, curve 2, connecting the results of calculation H10 (for zero water content) with H4 for 17 percent water by weight, appears to give a totally erroneous impression of the variation of residual stress with water content.

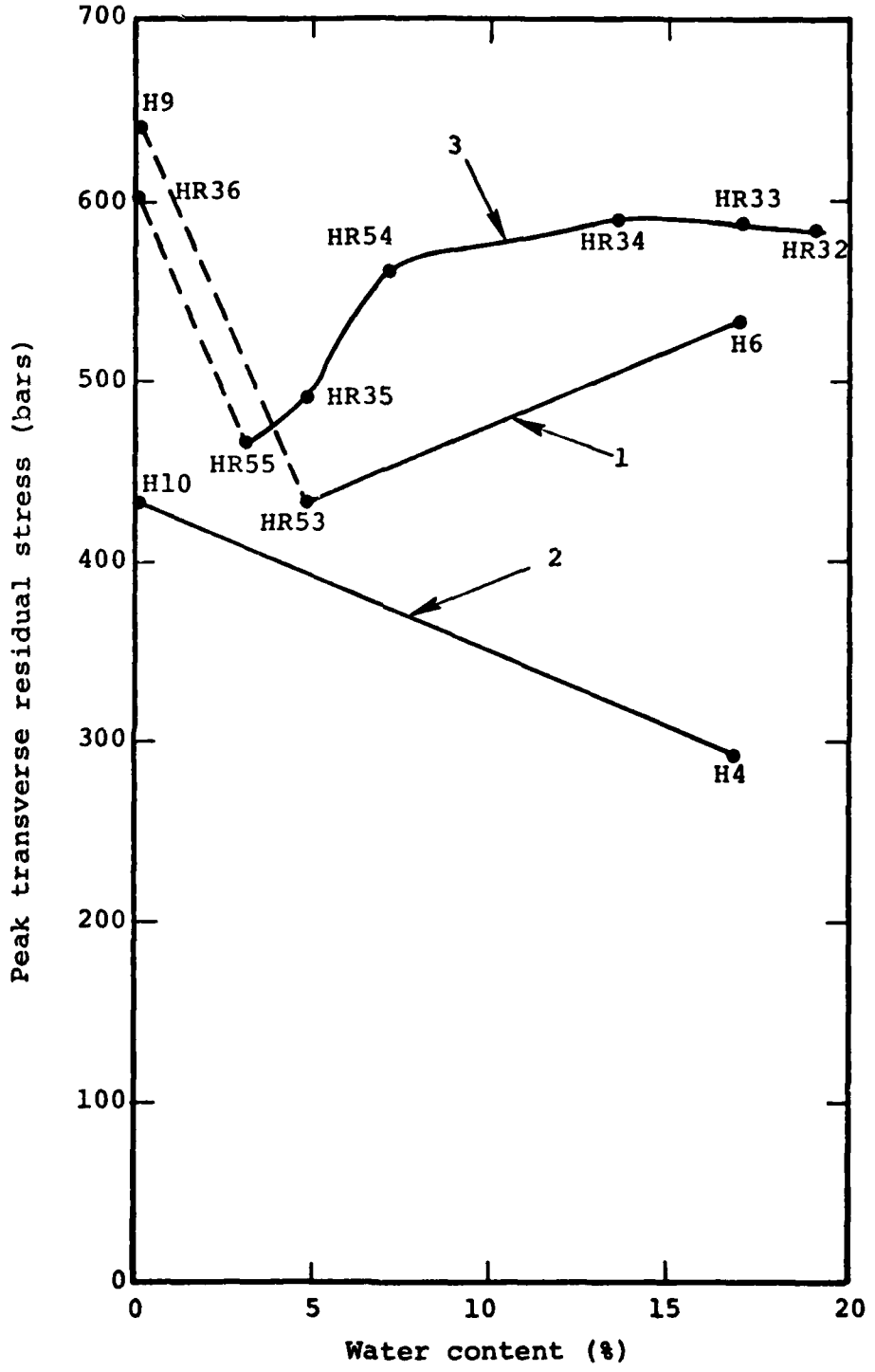

Figure 3 – Peak transverse residual stress vs. mass fraction of water.

The data points for zero water content on curves 1 and 3 (connected to the rest of the curves by dotted lines) do not appear to be consistent with the remainder of the parameter study which shows a general increase in peak residual stress with water content for low water contents. Numerically, the calculations for zero water content differ from the other calculations in that the TAMEOS scheme is not used. Mixing water with the dry tuff using TAMEOS generates an equation of state having releases very different from the dry tuff alone. It is not clear at this time why this influences the residual stress variation at low water contents.

Curve 3 of Figure 3 shows very little change in peak residual stress for mass fractions of water above 7 percent. However, one very important effect of water content was not included in this parameter study; the decrease in the shear strength of the rock due to increased water content. Results will be presented later in this report that show that decreasing strength decreases the peak residual stress dramatically. Thus, one must draw conclusions from the results of these calculations with care. The influence of water on equation of state has been included. The influence of water on rock strength has not. It may well be that the net effect of increasing water content will be a decrease in residual stress field around the cavity.

Figure 4 shows the dependence of residual stresses on the volume fraction of air-filled voids. The curve summarizes calculations H1, H6 and H8 and indicates that the peak residual stresses are greater for materials with less voids. The crushing up of these voids acts as a smoothing (dispersive) mechanism which may reduce the nonuniformity of the plastic loading. An argument has already been presented that it is this nonuniformity which causes residual stresses.

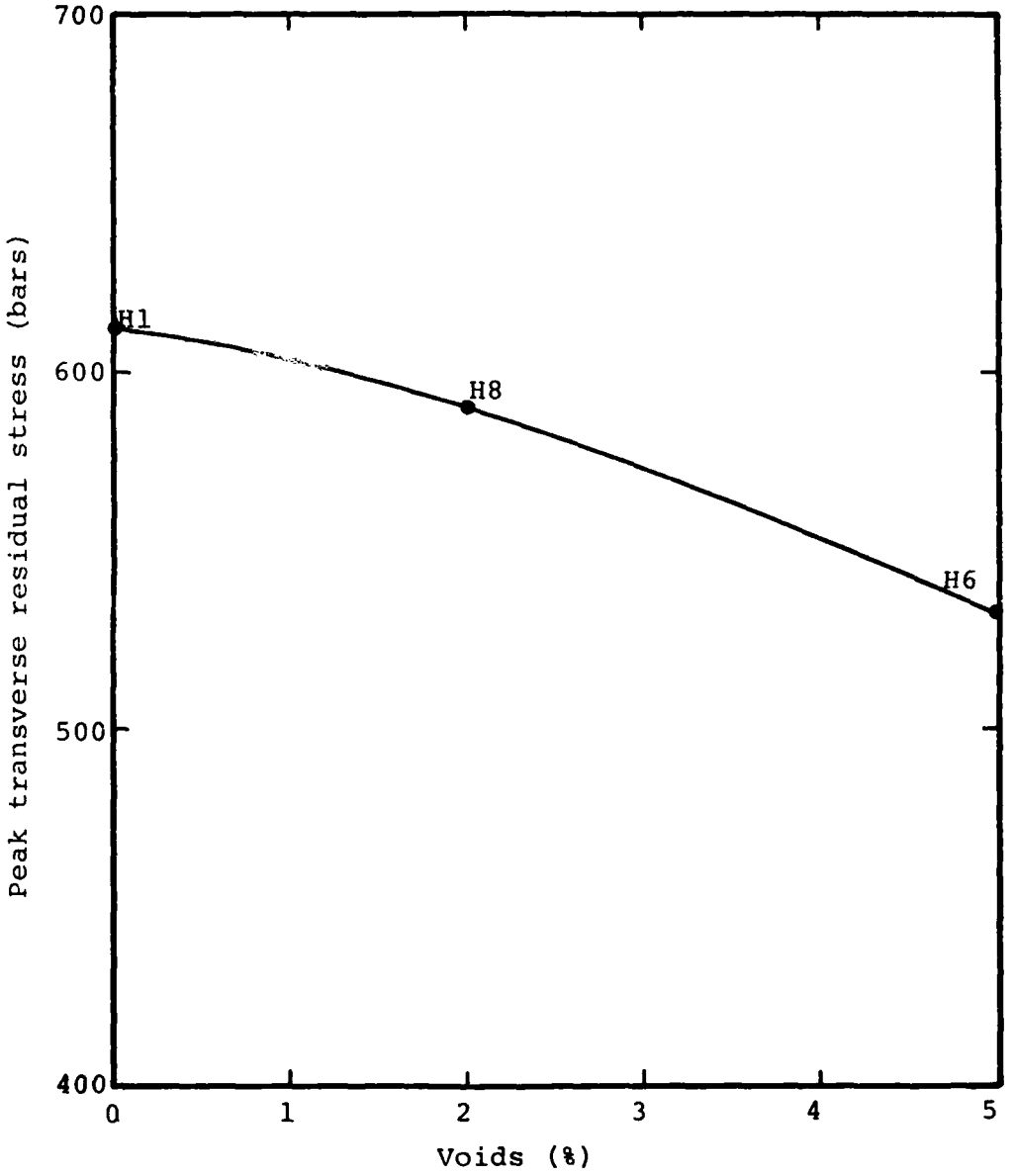

Figure 4 - Peak transverse residual stress vs air-filled voids.

Calculations 13 to 17 differ only slightly in air-filled voids. In order to compare other features of these calculations, we will assume that these calculations do not differ in this property. Figure 4 indicates that the difference between 1.2 and 1.6 percent air-filled voids is only 4 percent in transverse residual stress. Similarly, the difference in water contents among these calculations is only a small effect.

The comparison of calculations H11 and H27 shown in Figure 5 indicates that a higher crush pressure results in a larger residual stress. It reduces the smoothing effect by steepening the crush curve and by moving the crush curve into the higher stress regime. In a similar way, the increase in residual stresses due to the increase in elastic pressure shown in Figure 5 may be explained.

For all the nonsaturated materials studied, the maximum residual stresses were observed near the radial position corresponding to the end of the fully crushed region (where peak radial stress is equal to the crush pressure). Material loaded to above P_c unloads along its isentrope independent of the shape of the crush curve. However, material which was never fully crushed has an unloading path which depends on the shape of the crush curve and on the amount of loading it has been subjected to. This nonuniformity between load-unload paths for the materials near P_c leads to large final state gradients and is probably why the peak residual stress is located at the end of the fully crushed region.

2.3 SHEAR MODULUS

Curves 1, 2 and 3 of Figure 6 indicate that increasing the shear modulus results in an increase in peak transverse residual stress. Curve 4, the results of calculations HZ41, HZ49 and HZ50, however, show a very slight decrease in residual stress. The effect of shear modulus appears small, but is very difficult to decouple from the effect of varying zero pressure bulk modulus and sound speed which are related by

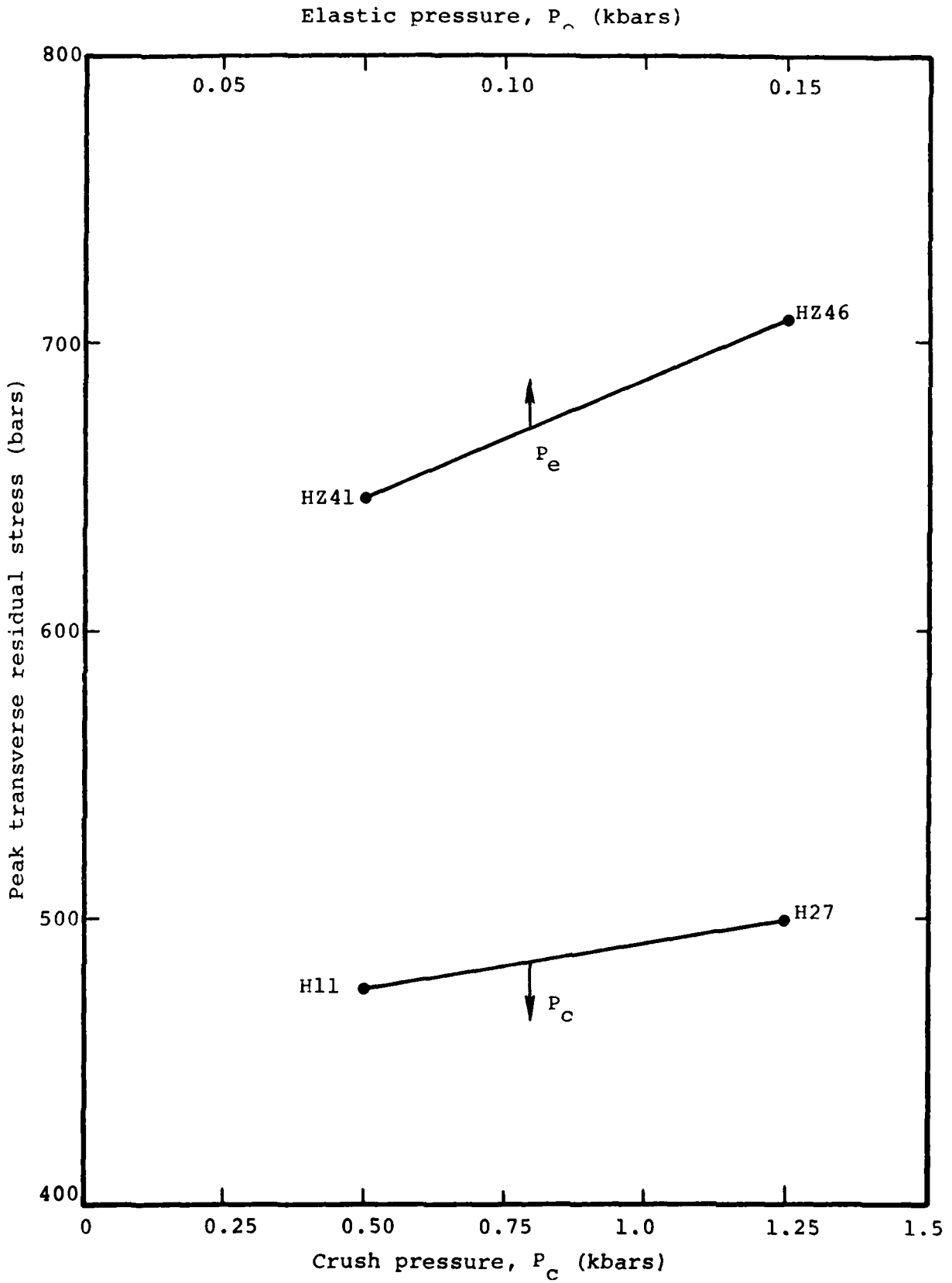

Figure 5 - Peak transverse residual stress vs crush pressure.

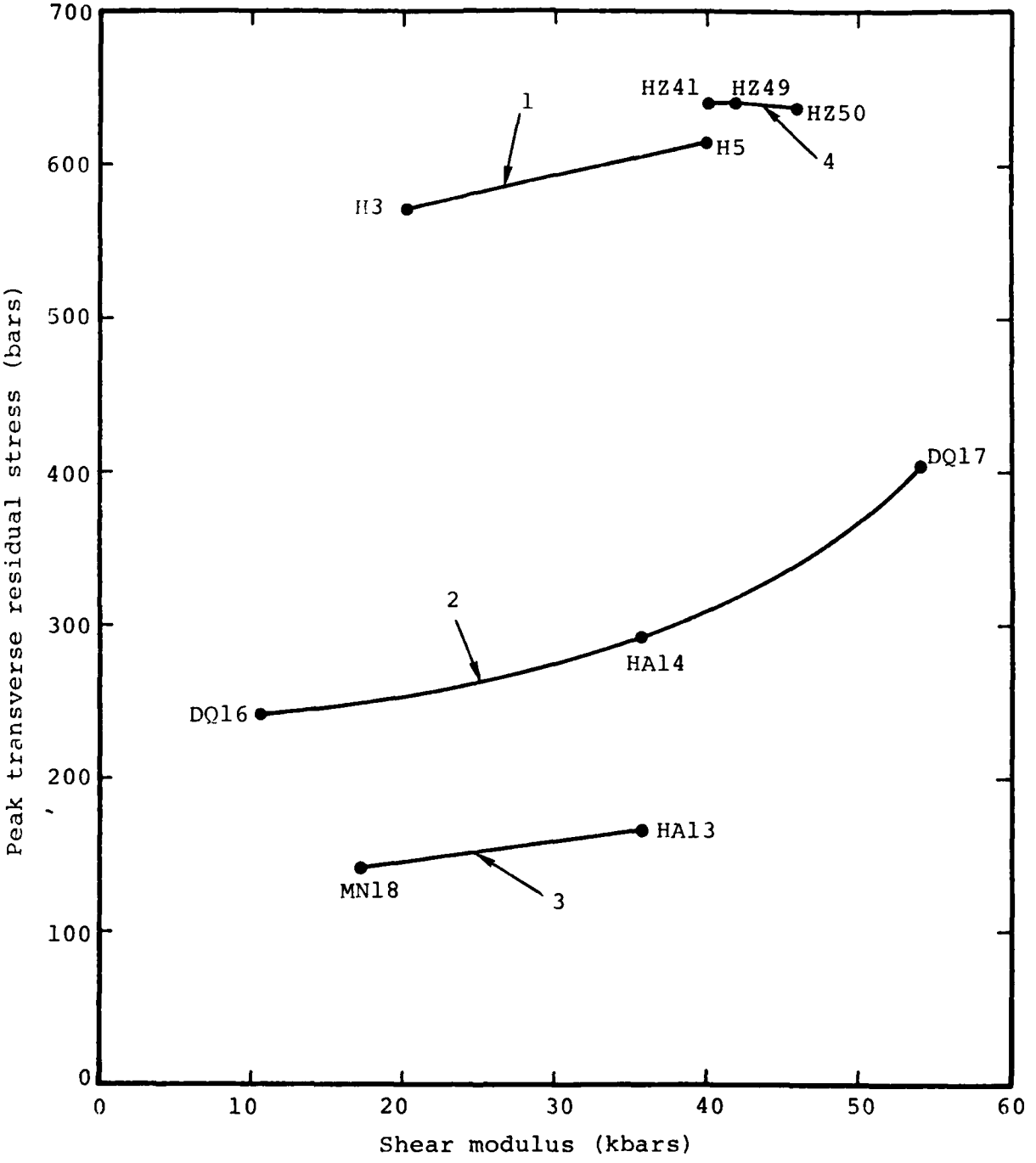

Figure 6 - Peak transverse residual stress vs shear modulus.

$$\rho_o C_o^2 = K_o + 4/3\ G$$

where

ρ = density
C = sound speed
K = bulk modulus
G = shear modulus

All calculations shown use a constant shear modulus to relate deviatoric stress history to strain rates. Thus, the major influence of increased shear modulus is, for the same strain history, to reach the von Mises failure surface, i.e., to behave plastically, more quickly. Residual stresses will be shown to be coupled very closely to the plastic behavior of the rock and to the failure surface.

2.4 FAILURE SURFACE

The material strength model used in SKIPPER requires that the principal stress be within the von Mises yield surface. This is equivalent, for spherical symmetry, to the radial deviatoric stress S_D satisfying the following inequality

$$|S_D| \leq 2/3\ Y \tag{5}$$

where Y is the yield strength (maximum stress difference) equivalent to twice the maximum shear strength. The non-associated flow rule is used for all calculations. Thus, whenever S_D, as calculated from the strain rates, becomes greater in absolute value than 2/3 Y, its magnitude is decreased to 2/3 Y. The yield strength Y, considered to depend both on pressure and energy, is given by

$$Y = \left[Y_o + Y_m \frac{P}{P_m}\left(2 - \frac{P}{P_m}\right)\right]\left(1 - \frac{e}{e_m}\right), \quad P < P_m, \; e < e_m \qquad (6a)$$

$$Y = \left(Y_o + Y_m\right)\left(1 - \frac{e}{e_m}\right), \quad P \geq P_m, \; e < e_m \qquad (6b)$$

$$Y = 0, \quad e \geq e_m \qquad (6c)$$

where

Y_o = cohesive strength

Y_m = maximum increase in Y due to pressure

P_m = pressure at which the maximum stress difference under triaxial compression $(Y_o + Y_m)$ is attained

e_m = melt energy

Here, P includes a scalar overburden pressure.

A comparison between calculations HR37 and HR33 shows that increasing the melt energy by over a factor of 2 decreases the peak transverse residual stress by only about 3 percent. Thus, e_m does not appear to be an important parameter.

Figure 7 shows four comparisons, all of which indicate that increasing the maximum yield strength $(Y_o + Y_m)$ increases the magnitude of the residual stresses. For the analogy of torsion of an ideal plastic cylinder, the magnitude of the peak residual stress can be shown analytically to be linearly proportional to the yield stress (see Rimer[3]). Thus, the strong dependence between strength and residual stresses around a nuclear cavity is not surprising.

The curves in Figure 7 are for different failure surfaces. Some have nonzero cohesive strengths, while others do not. Figure 8 shows the effect of varying Y_o while maintaining the maximum yield strength $(Y_o + Y_m)$ constant at

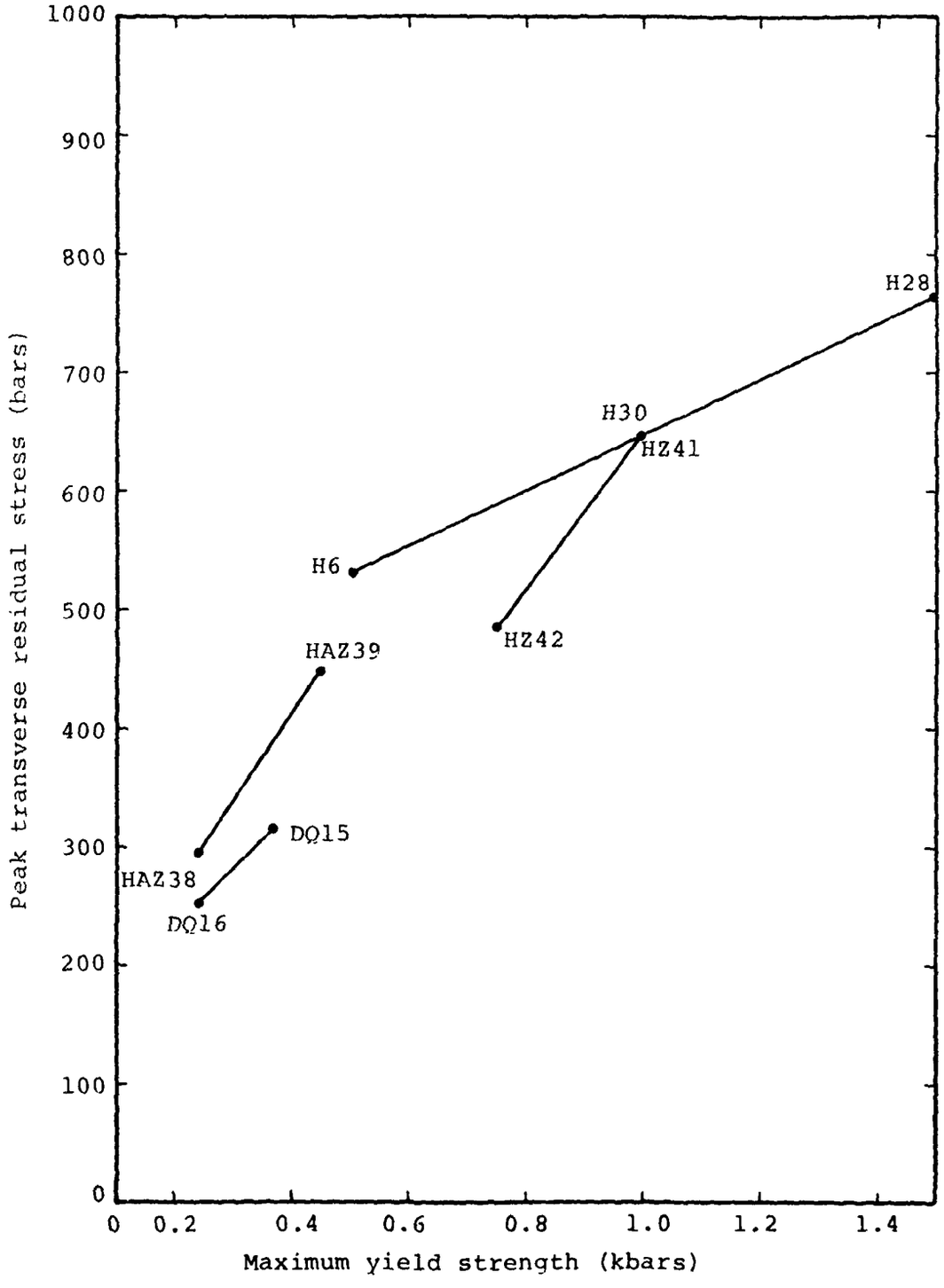

Figure 7 - Peak transverse residual stress vs maximum yield strength ($Y_o + Y_m$).

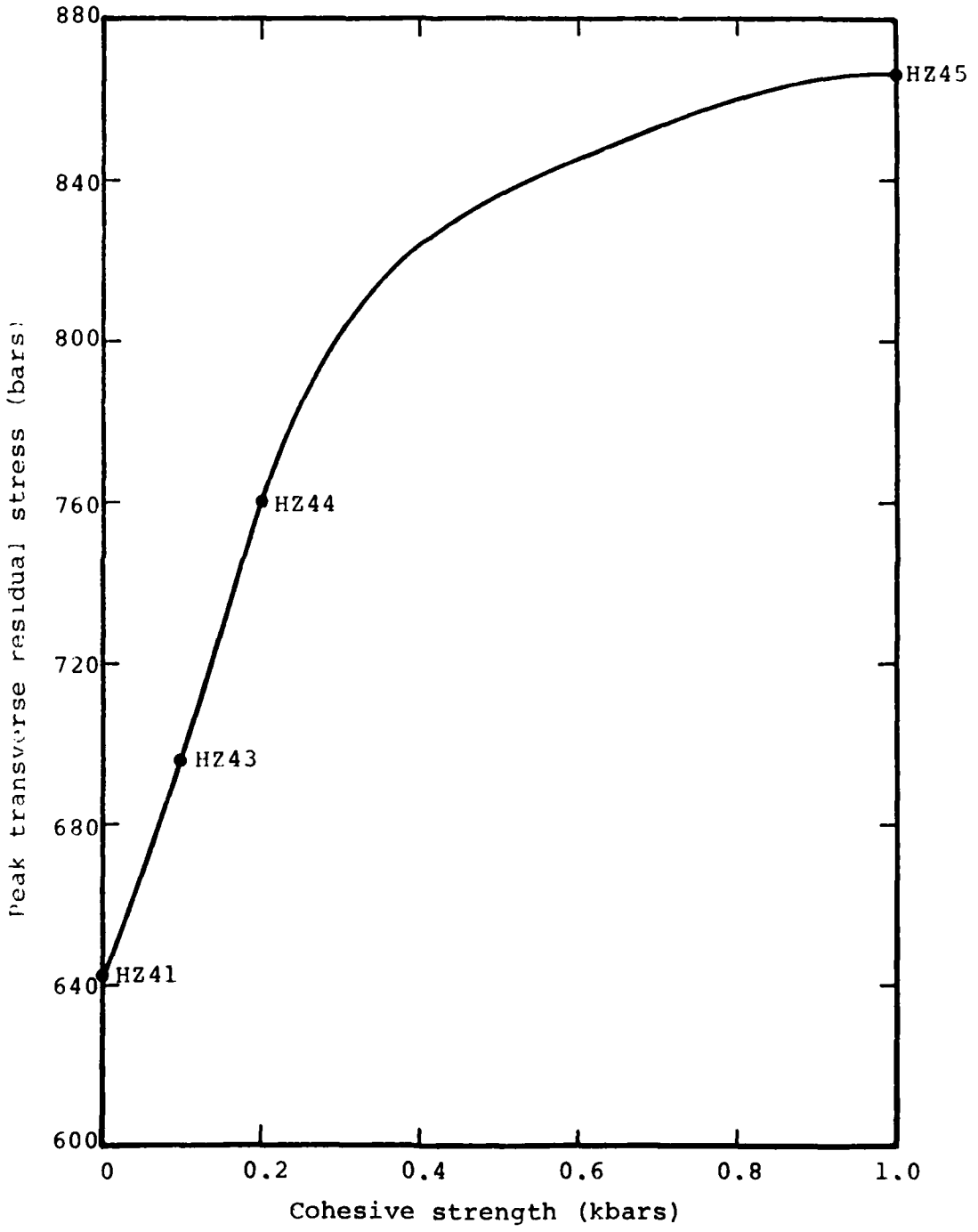

Figure 8 - Peak transverse residual stress vs cohesive strength (Y_o).

1 kbar. Increasing the proportion of Y_o in the yield strength increases the residual stresses since for any given pressure less than P_m, Y will be increased. The limiting case of no pressure dependence, $Y = Y_o$ (calculation HZ45) is shown for comparison.

2.5 DEPTH OF BURIAL

The depth of burial of the device is represented in this study by an overburden pressure which is added to the pressure computed from TAMEOS. One effect of overburden is to increase the work done term and therefore to increase the internal energy further during compression. The most important effect of overburden on residual stress is its influence on the failure surface given in Equation (6). Overburden is added onto the pressure, increasing the yield strength. Figure 9 shows the resulting increase in peak residual stress with overburden.

2.6 TENSION CRACKS

Calculations S20 through S24, for shale, use the modified Tillotson equation of state discussed in Rimer.[3] These calculations allow the material to crack in tension whenever a principal stress becomes greater than some maximum tensile stress. The crack is allowed to grow and subsequently close when the stress distribution becomes compressive. Figure 10 indicates that the higher the allowable stress in tension is made, i.e., the stronger the material in tension, the weaker the residual stress field around the cavity becomes. It appears that whenever tension cracks open in the rock and subsequently close, the residual stress membrane around the cavity is stronger than if no cracking occurred. Calculation S21 represents the effect of no cracking and corresponds to a tensile strength greater than or equal to 27 bars.

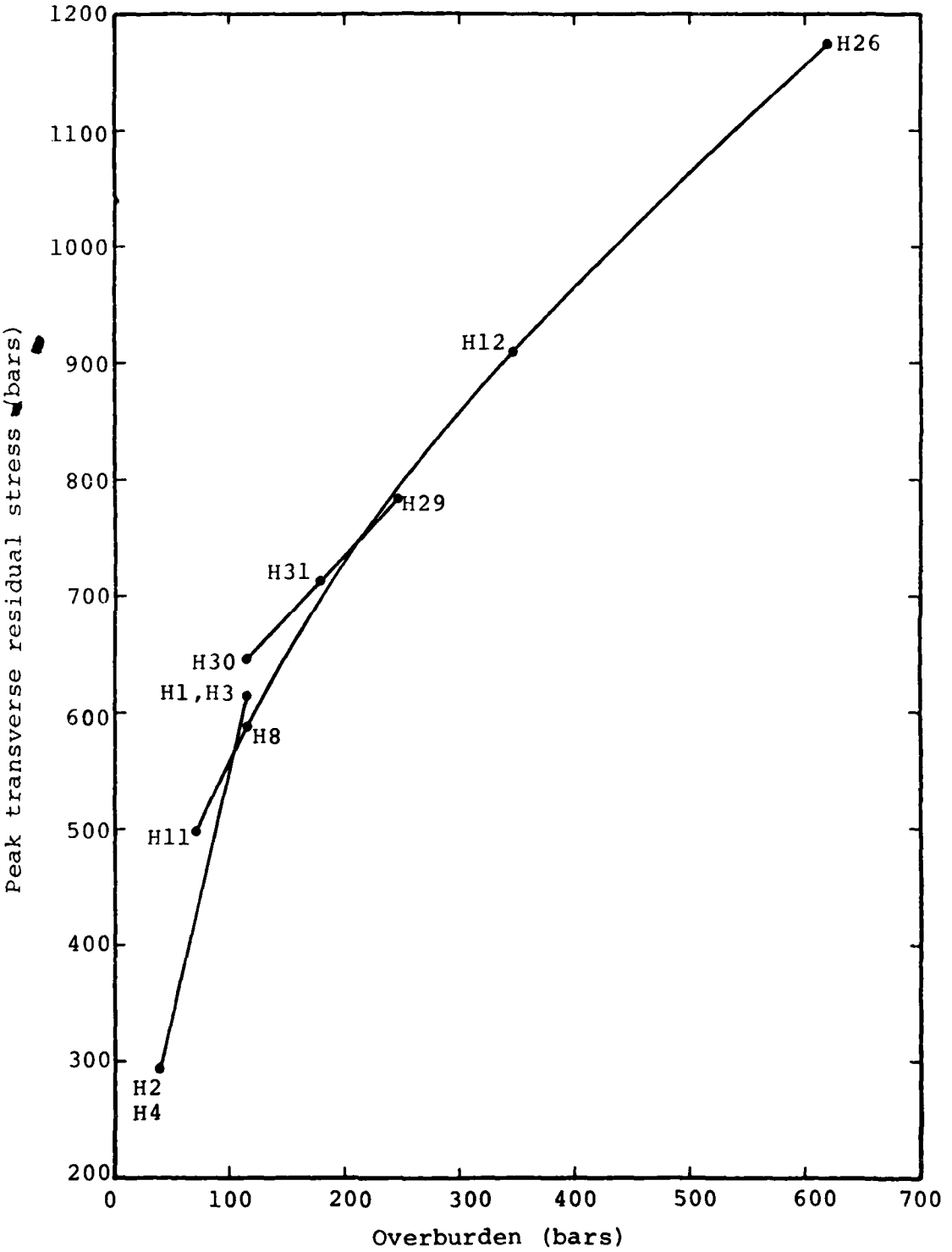

Figure 9 - Peak transverse residual stress vs overburden.

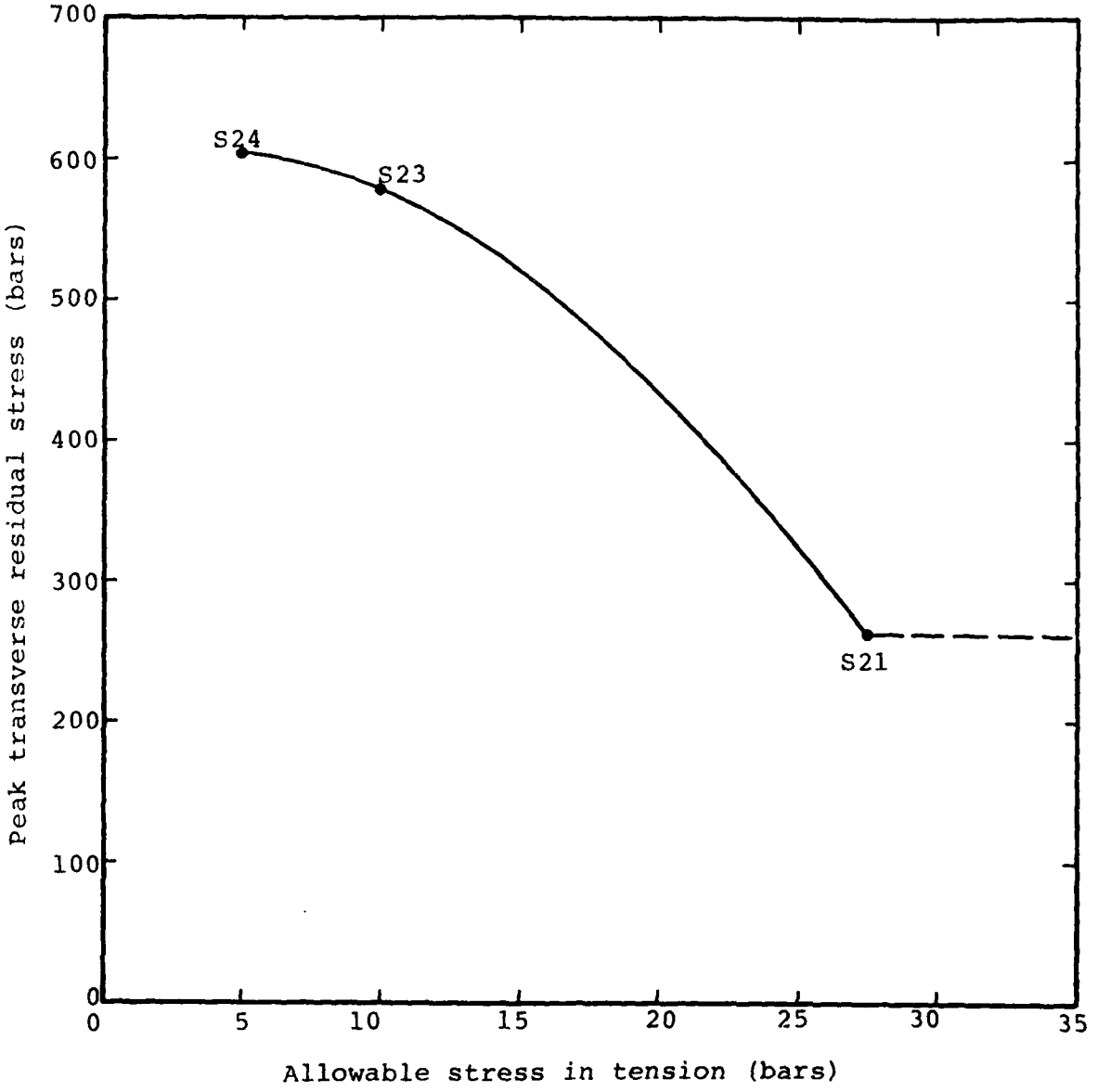

Figure 10 - Peak transverse residual stress vs tensile strength.

The above results may be explained in terms of distribution of stress around the cavity. When tensile cracks are opened, the cavity region where residual stresses form is essentially decoupled from the propagating stress waves. Thus, cracking increases the nonuniformity of the stress distribution in this region. Since rock has been loaded into the plastic regime, on unloading, greater residual stresses should be present.

3. THE EFFECT OF MATERIAL PROPERTIES ON CAVITY RADIUS

Final cavity radii are presented in Table 1 for a nominal device yield of 20 tons. From these, cavity radii may be obtained for other yields using $W^{1/3}$ scaling. The effect of material properties on cavity radius is studied here and a correlation made with residual stresses. The effect of cavity source modeling has been discussed in Chapter 2.

3.1 WATER CONTENT, AIR-FILLED VOIDS AND SHEAR MODULUS

Figure 11 indicates that increasing the water content decreases the final cavity radius. An effective stress law would be expected to give an increase rather than the decrease seen in Figure 11. However, the decrease in strength due to increased water content is not included in the calculations used for this study. Therefore, the results shown must be due to the complicated releases from high pressure states given by TAMEOS for water-rock mixtures.

Increasing air-filled voids results in the increase in cavity radius shown in Figure 12. When the voids are crushed up, the cavity has more room to expand. Increasing the crush pressure p_c results in less void crushup. Therefore, as shown in Figure 13, cavity radii are smaller. Similarly, a higher elastic pressure p_e results in less permanent crushup and smaller cavity radius.

Figure 14 indicates that higher shear modulus materials give smaller cavity radii.

3.2 FAILURE SURFACE, DEPTH OF BURIAL AND TENSION CRACKS

The modeling of the yield surface was discussed in Section 2.4. Figure 15 shows that yield strength is the

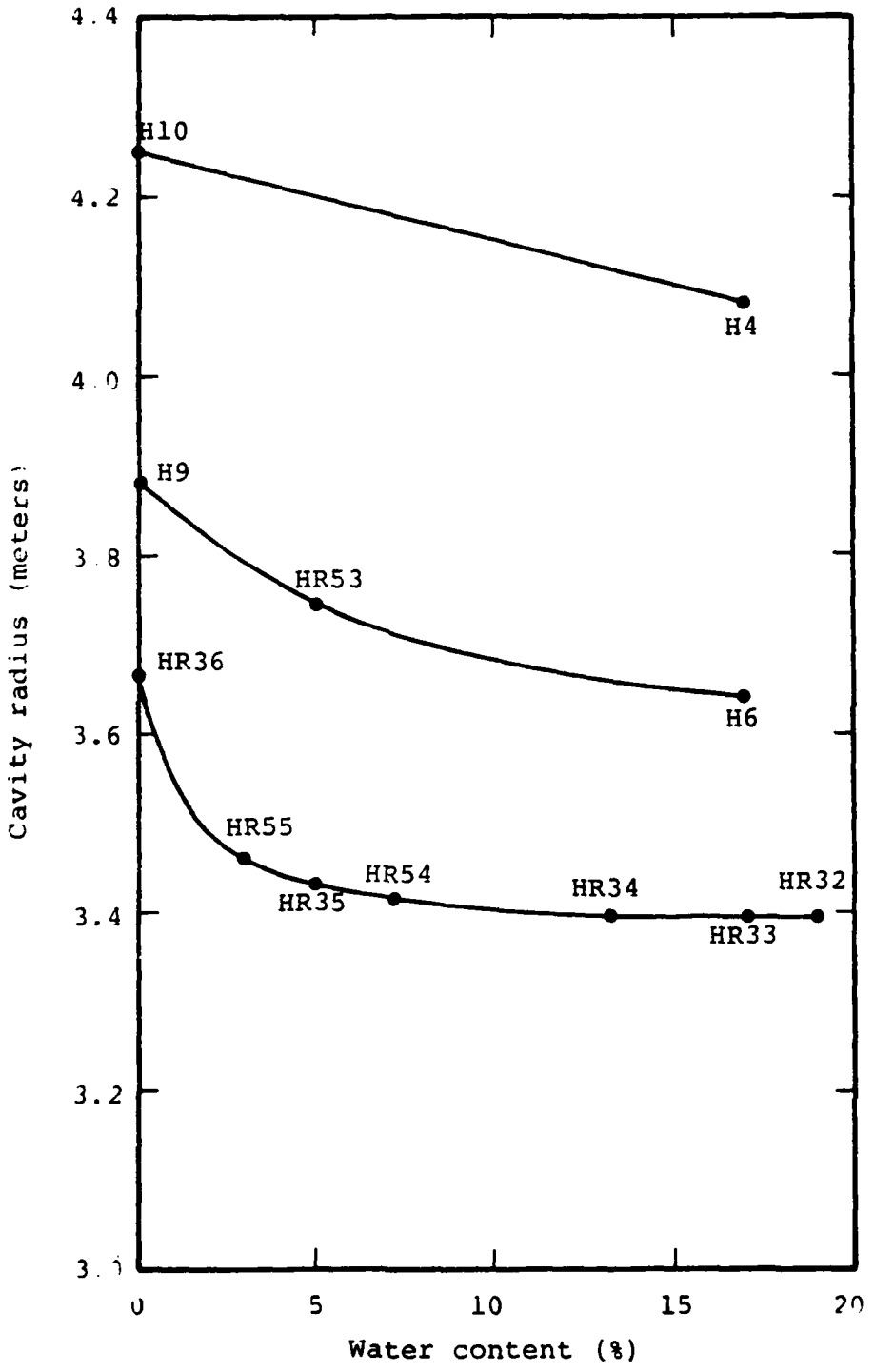

Figure 11 - Final cavity radius vs mass fraction of water.

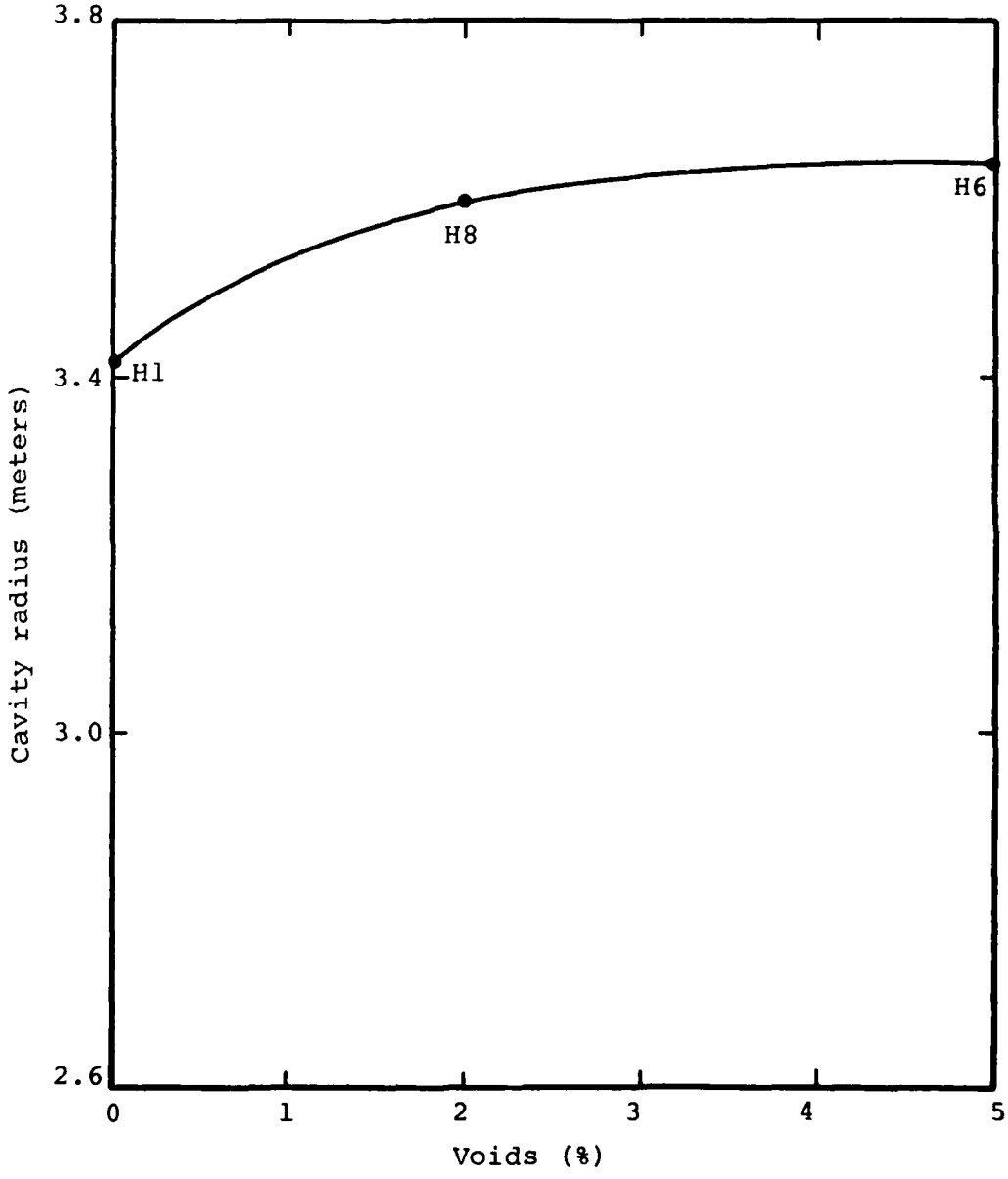

Figure 12 - Final cavity radius vs air-filled voids.

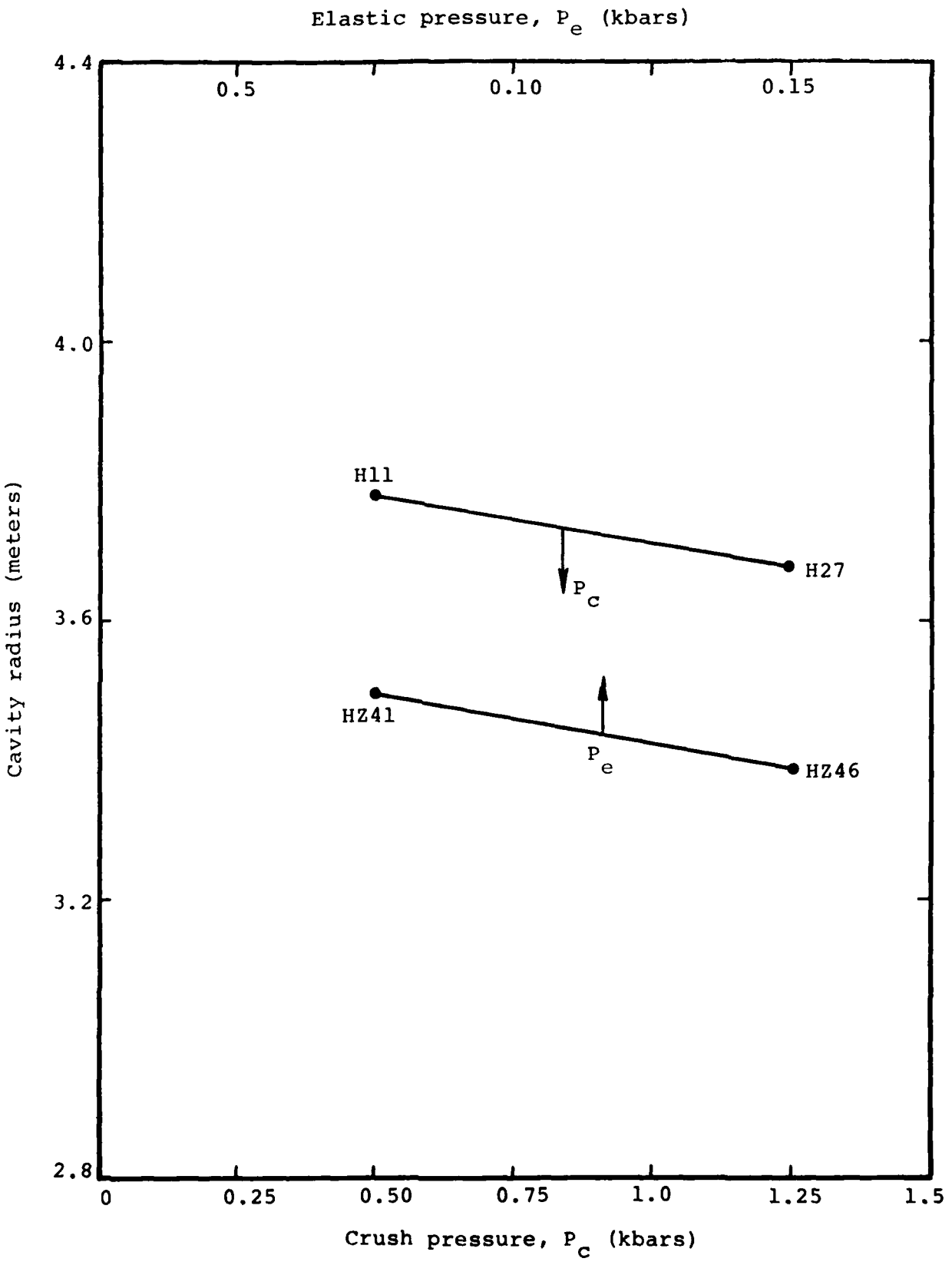

Figure 13 - Final cavity radius vs crush pressure.

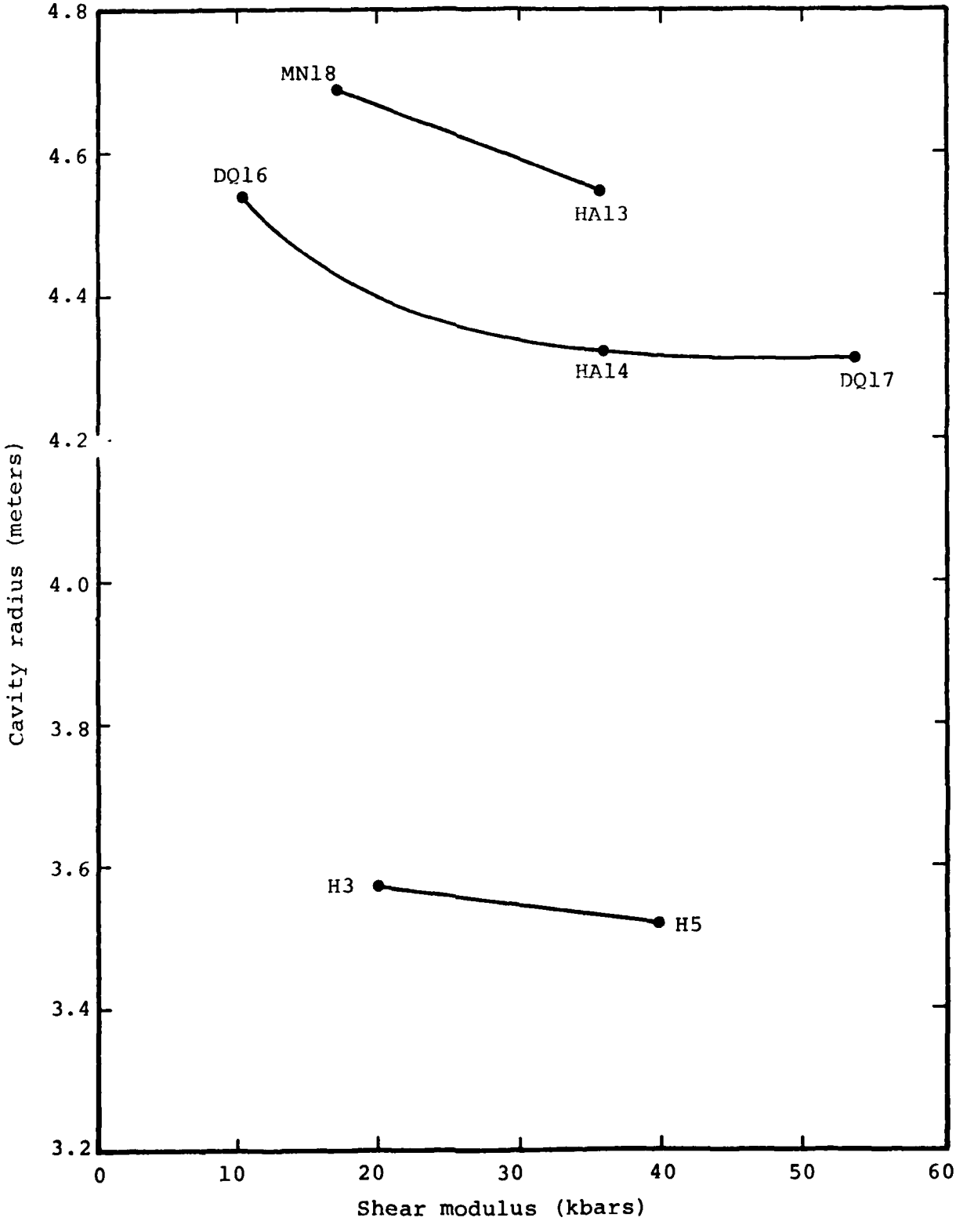

Figure 14 - Final cavity radius vs shear modulus.

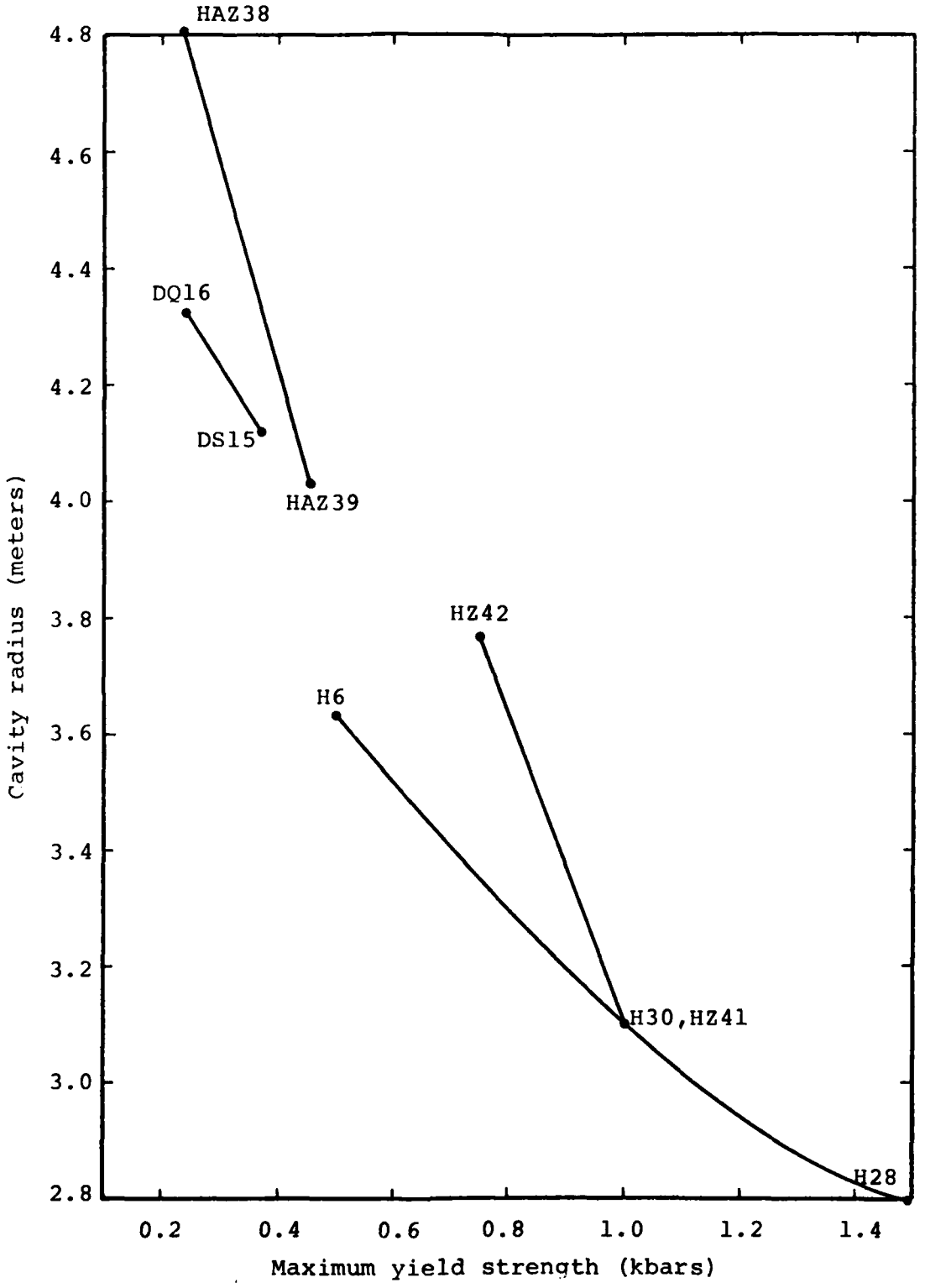

Figure 15 - Final cavity radius vs maximum yield strength ($Y_o + Y_m$).

material property of greatest influence on cavity radius. Strong materials give small cavities. This is in agreement with earlier work by Allen and Duff.[14] Figure 16 indicates that the cohesive strength Y_o is very influential in determining final cavity radius. An argument may be made that at early times, the cavity pushes out so strongly that it does not even notice the strength of rock around it. However, when the surrounding rock has unloaded to lower stresses, the strength at low pressure is predominant in slowing down and finally stopping cavity growth. If the rock has negligible strength, the cavity will continue expanding forever. In all calculations, it is noticed that the cavity expands beyond its final radius and then reverses its motion. It is during this time period that the residual stresses reach their final magnitudes.

Increased depth of burial, for the modeling used, results in higher yield strength at lower dynamic pressures. Therefore, increasing overburden pressure results in decreases in cavity radii. These are quite close to those predicted by the CEP $h^{-1/4}$ relationship as shown in Figure 17. Actually, the calculated cavity radius does not decrease quite as fast as the CEP formula suggests. An $h^{-1/5}$ dependence is in better agreement with the calculational results.

Figure 18 shows no clear trend between allowable tension stress and cavity radius.

3.3 CAVITY RADIUS AND PEAK RESIDUAL STRESS

Figure 19 is a plot of peak transverse residual stress vs cavity radius; each point in the plot represents one of the calculations of Table 1. The trend is clear. A larger cavity radius indicates a smaller residual stress. When variations in an individual material property are examined, this trend is

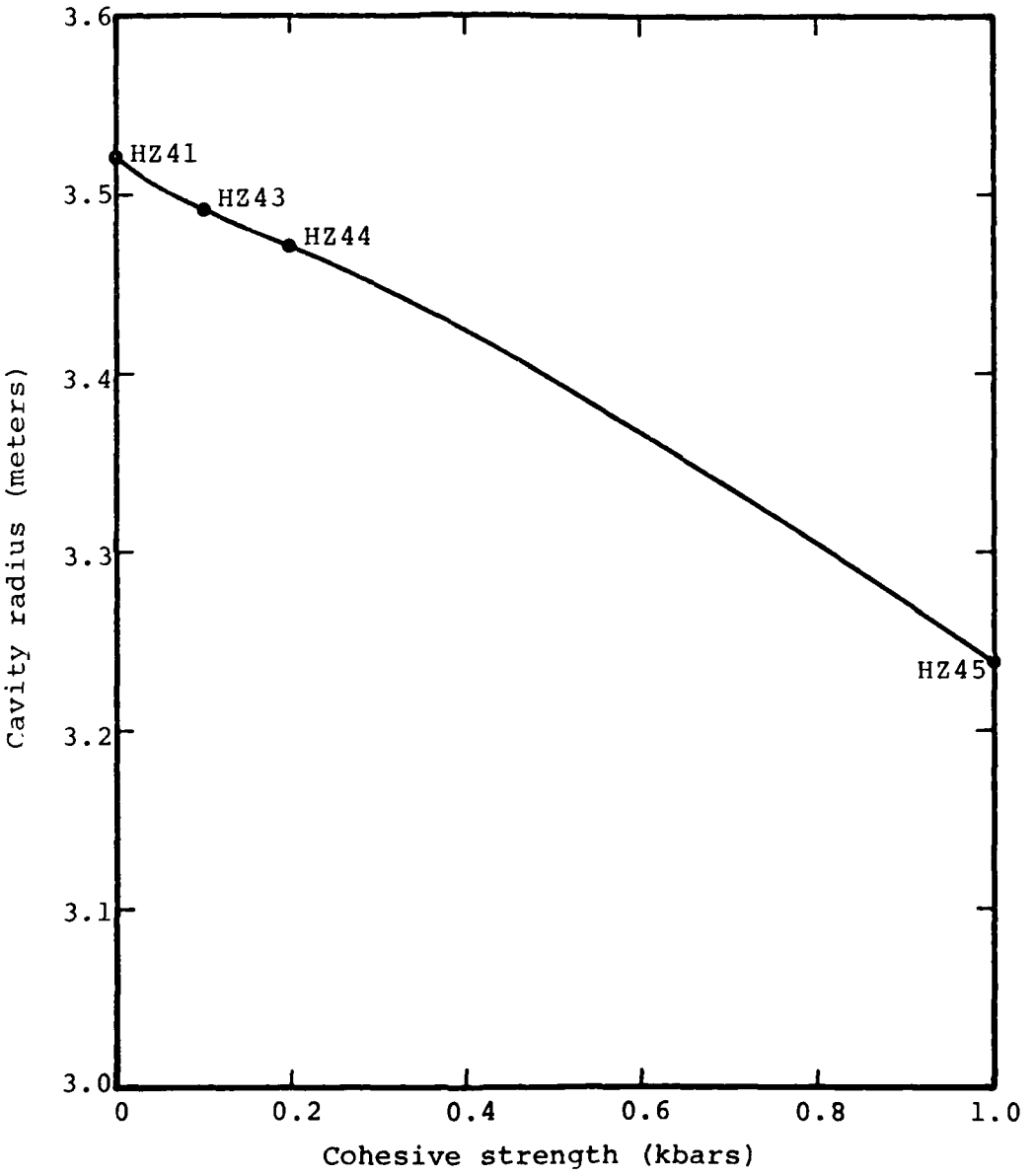

Figure 16 - Final cavity radius vs cohesive strength (Y_o).

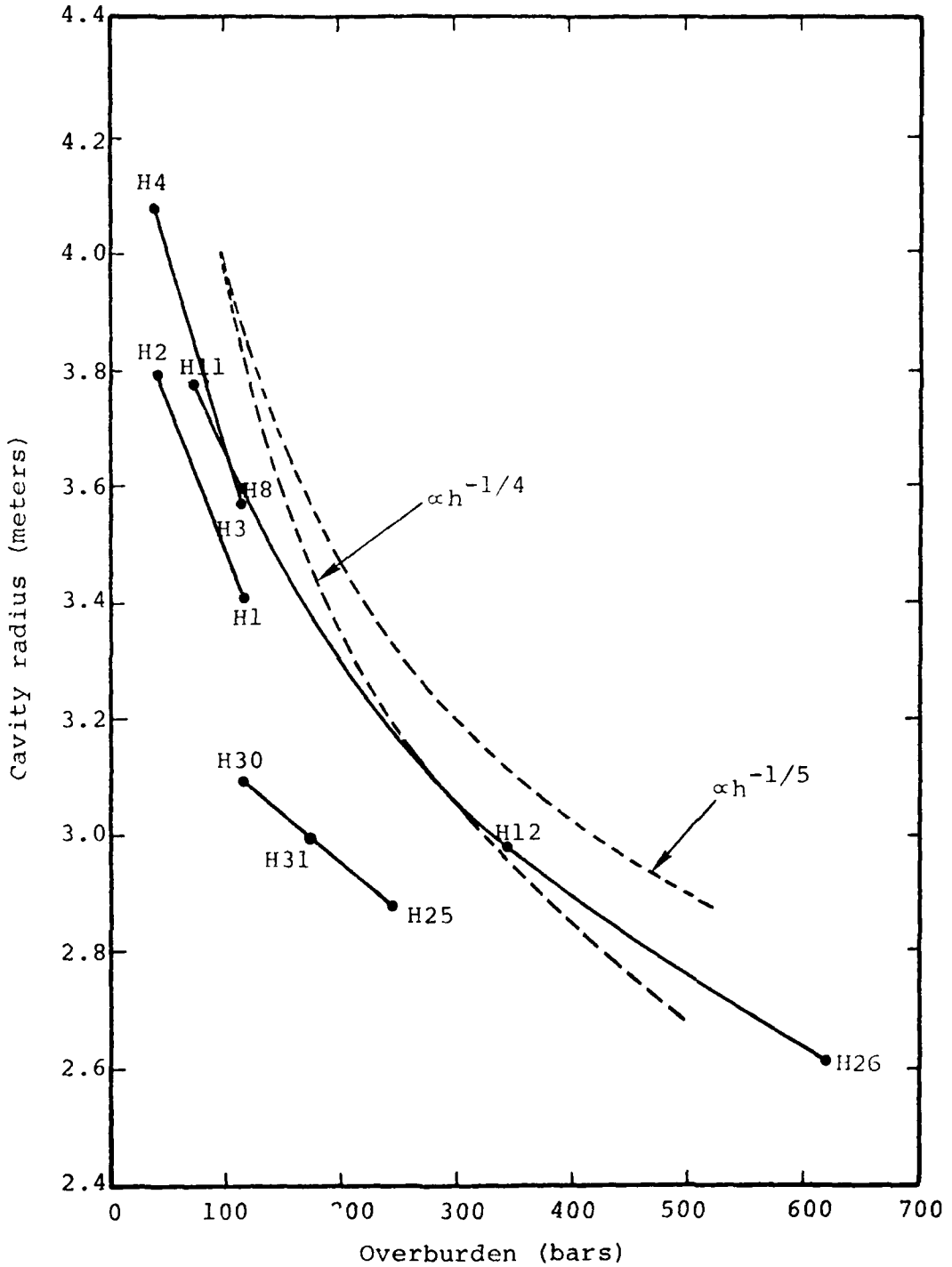

Figure 17 - Final cavity radius vs overburden. (Curves showing variations with depth of burial of $h^{-1/4}$ and $h^{-1/5}$ are included for reference.)

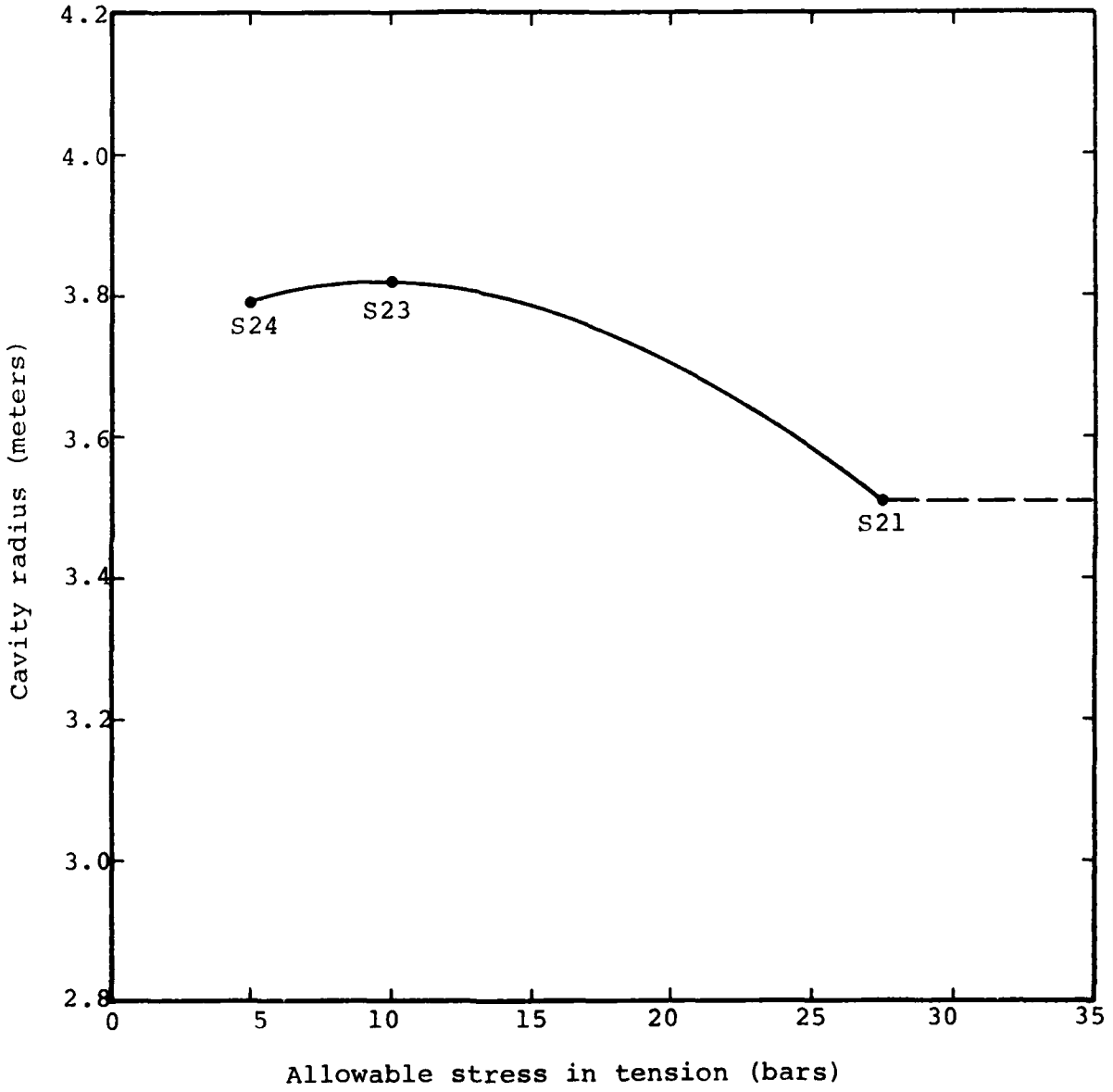

Figure 18 - Final cavity radius vs tensile strength.

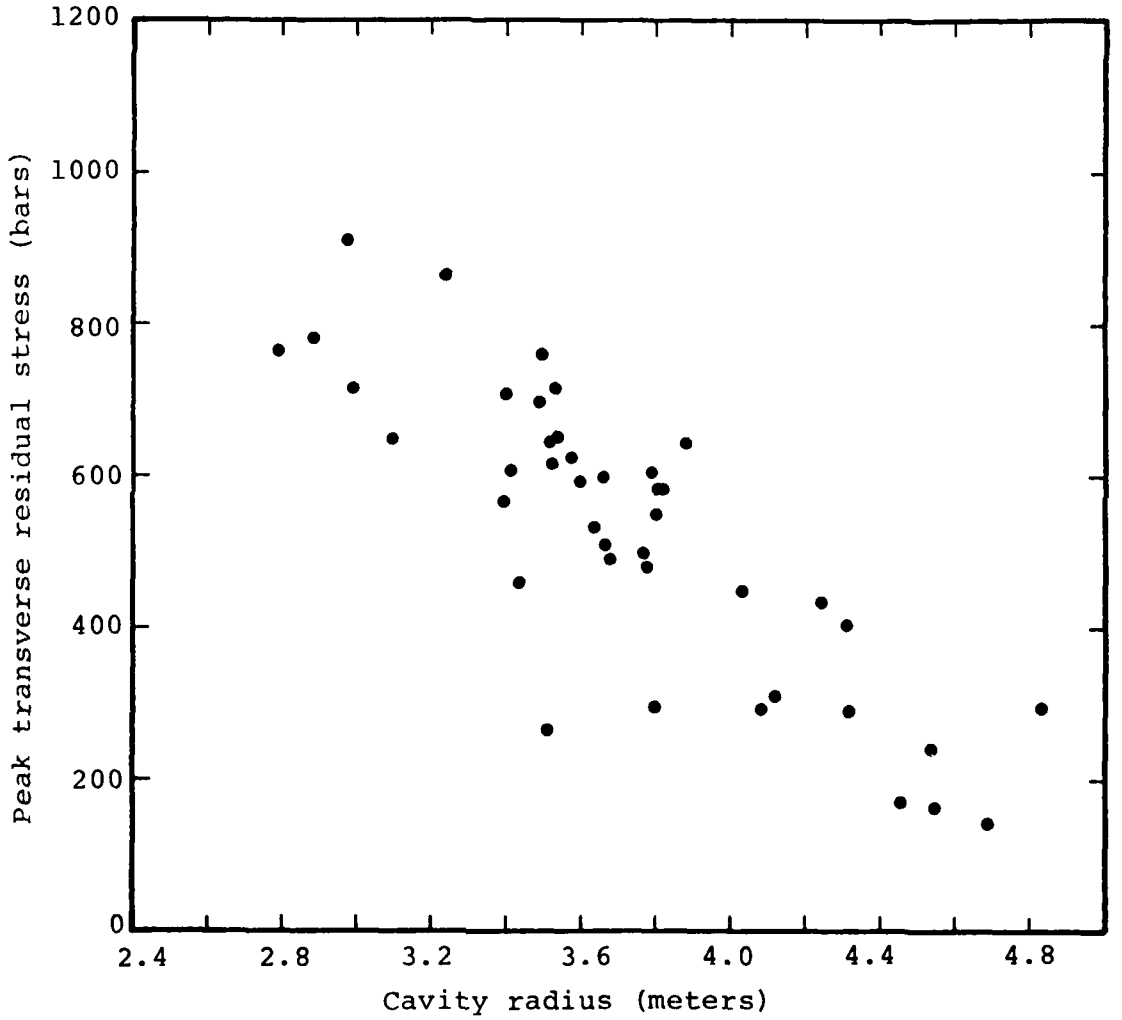

Figure 19 - Peak transverse residual stress vs final cavity radius for calculations of Table 1.

seen for all properties with the exception of allowable tensile strength where no clear trend is evident.

It has been noted that the residual stresses reach their final values at about the time of cavity formation. The cavity generally overexpands and rebounds inward. At this time, the rock is squeezed together, due to convergence effects, giving rise to the large hoop stresses (transverse residual stresses). This convergence effect is greatest for smaller cavity radii.

REFERENCES

1. Ellis, William L., USGS, letter to J. LaComb, December 1975.

2. Duff, R. E., K. H. Lie and W. Z. Savage, "Residual Stress Fields in the Vicinity of an Explosion-Produced Cavity and Related Topics," Systems, Science and Software report, SSS-R-75-2533 (submitted to DNA) June 1975.

3. Rimer, N., "The Influence of Material Properties on the Magnitude of Residual Stresses Around a Nuclear Cavity," Systems, Science and Software report, SSS-R-75-2658 (submitted to DNA) June 1975.

4. Rimer, N., J. M. Walsh and J. T. Cherry, "Teleseismic Body Wave Magnitudes as Predicted from Near Field Ground Motion Calculations for Four Nevada Events," Systems, Science and Software report, SSS-R-75-2464 (submitted to DNA) October 1974.

5. Cherry, J. T., A. J. Good and K. G. Hamilton, "Near Field Calculations for Seismic Predictions," Systems, Science and Software final report, SSS-R-73-1605 (submitted to DNA) April 1973.

6. Cherry, J. T., N. Rimer and W. O. Wray, "Seismic Coupling from a Nuclear Explosion: The Dependence of the Reduced Displacement Potential on the Nonlinear Behavior of the Near Source Rock Environment," Systems, Science and Software report, SSS-R-76-2742 (submitted to ARPA) September 1975.

7. Bache, T. C., J. M. Savino, N. Rimer and W. Z. Savage, "A Preliminary Comparison of the Teleseismic Magnitude of Explosions at Rainier Mesa to Those in Dry Tuff at Yucca Flat," Systems, Science and Software report, SSS-R-75-2517 (submitted to DNA) Decmeber 1974.

8. Allen, R. T., DNA sponsored discussion at S^3 of earth motion calculations, November 12, 1975.

9. Bjork, R. L., private communication (1975).

10. Schroeder, R. C., "A Comparison of Initial Conditions for Nuclear Explosion Calculations," Lawrence Livermore Laboratory report, UCRL-51671, October 1974.

11. Laird, D., "A Chemical Equilibrium Equation of State for Saturated Tuff," Systems, Science and Software report, SSS-R-75-2740 (submitted to DNA) October 1975.

12. Bjork, R. L. and M. L. Gittings, "Wave Generation by Shallow Underwater Explosions," Systems, Science and Software report, 3SR-1008 (submitted to DNA) 1972.

13. Riney, T. D., J. K. Dienes, G. A. Frazier, S. K. Garg, J. W. Kirsch, D. H. Brownell and A. J. Good, "Ground Motion Models and Computer Techniques," Systems, Science and Software final report, 3SR-1071 (submitted to DNA) April 1972.

14. Allen, R. T. and R. E. Duff, "Effect of Material Properties on Cavity Size from an Underground Explosion," Nuclear Applications, Vol. 6, June 1969.

DISTRIBUTION LIST

DEPARTMENT OF DEFENSE

Defense Nuclear Agency
ATTN: SPTD, T. Kennedy
4 cy ATTN: TITL

Defense Technical Information Center
12 cy ATTN: DD

Field Command
Defense Nuclear Agency
ATTN: FCTT, W. Summa
ATTN: FCTT, G. Ganong
ATTN: FCT, P. Oppedahl
3 cy ATTN: FCTK, B. Ristvet
3 cy ATTN: FCTK, C. Keller

Field Command Test Directorate
Defense Nuclear Agency
ATTN: FCTC, J. Lacomb

DEPARTMENT OF ENERGY

Department of Energy
Nevada Operations Office
ATTN: R. Newman

Desert Research Institute
ATTN: D. Schulke Sec Off for C. Case
ATTN: D. Schulke Sec Off for P. Fenske

DEPARTMENT OF ENERGY CONTRACTORS

Lawrence Livermore National Lab
ATTN: B. Hudson
ATTN: J. Shearer
ATTN: L-209, G. Higgins
ATTN: R. Terhune
ATTN: L. Makague

Los Alamos National Lab
ATTN: J. Wing
ATTN: E. Jones
ATTN: R. Brownlee
ATTN: F. App
ATTN: T. Kunkle
ATTN: B. Travis

DEPARTMENT OF ENERGY CONTRACTORS (Continued)

Sandia National Lab
ATTN: C. Mehl
ATTN: C. Smith
ATTN: A. Chabai

OTHER GOVERNMENT AGENCIES

Department of the Interior
U.S. Geological Survey
ATTN: R. Carroll
ATTN: A. Fernald

DEPARTMENT OF DEFENSE CONTRACTORS

California Research & Technology, Inc
ATTN: M. Rosenblatt

Kaman Tempo
ATTN: DASIAC

Pacific-Sierra Research Corp
ATTN: H. Brode

Pacifica Technology
ATTN: D. Patch

Physics International Co
ATTN: D. Mumma
ATTN: E. Moore

R & D Associates
ATTN: P. Haas

SRI International
ATTN: A. Florence

Systems, Science & Software, Inc
ATTN: C. Dismukes
ATTN: R. Duff
4 cy ATTN: N. Rimer


DAT
ILM